



NATIONAL ADVISORY COMMITTEE FOR AERONAUTICS

TECHNICAL NOTE 3794

DRAG INTERFERENCE BETWEEN A POINTED CYLINDRICAL BODY
AND TRIANGULAR WINGS OF VARIOUS ASPECT RATIOS

AT MACH NUMBERS OF 1.50 AND 2.02

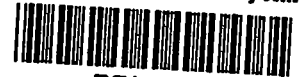
By Elliott D. Katzen and George E. Kaattari

Ames Aeronautical Laboratory
Moffett Field, Calif.

AFMDC
TECHNICAL LIBRARY
AFL 2811



Washington
November 1956



TECHNICAL NOTE 3794

DRAG INTERFERENCE BETWEEN A POINTED CYLINDRICAL BODY

AND TRIANGULAR WINGS OF VARIOUS ASPECT RATIOS

AT MACH NUMBERS OF 1.50 AND 2.02¹

By Elliott D. Katzen and George E. Kaattari

SUMMARY

In order to investigate the effects of drag interference on wing-body combinations, tests were conducted at Mach numbers of 1.50 and 2.02 with a pointed cylindrical body, with six triangular wings having aspect ratios from 0.67 to 4.00, and with the wings and the body in combination. Experimental drag results were obtained for a nominal angle-of-attack range of $\pm 5.5^\circ$ and a constant Reynolds number of 5.5 million based on the body length. The characteristics of the body, the wings, the combinations, and the wing-body interference were calculated from the available theories and compared with the experimental results.

The minimum drag coefficients of the body alone, as calculated by the method of characteristics with laminar and turbulent skin-friction coefficients added for the body in a smooth condition and with fixed transition, were in good agreement with the experimental values. The drag rise with angle of attack, as calculated by the method of NACA Rep. 1048, 1951, was much lower than the experimental drag rise of the smooth body, but was in fair agreement with that of the body with transition fixed. The data indicate that the transition point on the smooth body moved forward with increasing angle of attack, causing the skin friction to increase. In general, the predicted minimum drag coefficients of the wings (which included an estimate of the skin friction) were greater than the experimental values. The predicted minimum drag coefficients of the wing-body combinations were in good agreement with the experimental values. The better agreement for the combinations than for the wings alone was a result of the relatively greater accuracy in the calculation of the body drag which constitutes a large percentage of the combination drag.

Calculation of the pressures at zero angle of attack on the wings in the presence of the body by the method of NACA RM A9E19, 1949, indicated that the interference pressure drag was small for the present wing-body combinations if the wing alone were defined as the exposed half wings

¹Supersedes recently declassified RM A51C27 by Elliott D. Katzen and George E. Kaattari, 1951.

brought together. The experimental results indicated that the drag interference was principally the result of fixing transition by adding a wing.

INTRODUCTION

This report is the second of a series on interference effects between triangular wings of various aspect ratios and a pointed cylindrical body. The first report (reference 1) described the lift and pitching-moment interference; the present report is concerned primarily with the total drag interference, which is defined as the difference between the wing-body-combination drag force and the sum of the body alone and wing alone (exposed half wings brought together) drag forces.

Nielsen and Matteson (reference 2) have presented a method of calculating the drag interference on a wing in the presence of a circular cylindrical body. The purpose of the present report is to extend the study of interference to include a comparison of experimentally determined drag-interference forces with values calculated by the method of reference 2 (with skin-friction effects taken into account) for a series of triangular wing-body combinations, and to present a comparison of the experimental and calculated drag results for the body and the wings alone and in combinations.

NOTATION

a	local body radius, in.
a_{\max}	maximum body radius, in.
A	wing aspect ratio
A_p	plan-form area of body, sq in.
\bar{c}	mean aerodynamic chord $\left(\frac{2}{3} c_r\right)$, in.
c_{d_c}	cross-flow-section drag coefficient of a circular cylinder
c_r	wing apex chord, in.
C_D	total drag coefficient based on total wing-plan-form area for wings and combinations and on base area for body
	$\left(C_D = \frac{D}{qS} \text{ or } C_D = \frac{D}{q a_{\max}^2}\right)$
ΔC_D	increment in drag coefficient due to lift $\left(C_D - C_{D_{\min}}\right)$

$C_{D_{min}}$	total minimum drag coefficient
C_{D_p}	pressure drag coefficient
C_{D_f}	skin-friction drag coefficient
C_f	skin-friction coefficient based on wetted area
$C_{f_{turb}}$	skin-friction coefficient for turbulent flow at Reynolds number based on average chord of total wing for wing alone, on body length for body alone, and on average chord of exposed wing for the wing on the body
$C'_{f_{lam}}$	skin-friction coefficient for laminar flow at Reynolds number based on average length of laminar area
$C'_{f_{turb}}$	skin-friction coefficient for turbulent flow at Reynolds number based on average length of laminar area
C_L	lift coefficient based on total wing-plan-form area for wings and combinations and on base area for body $\left(\frac{L}{qS} \text{ or } \frac{L}{q\pi b_{max}^2} \right)$
D	drag force, lb
ΔD	increment in drag force due to lift, lb
$\frac{D_{WB} + D_{BW}}{D_B + D_W}$	total drag-interference ratio $\left(\frac{D_{WB} + D_{BW}}{D_B + D_W} = \frac{D_C}{D_B + D_W} - 1 \right)$
E	complete elliptic integral of second kind of modulus $\sqrt{1 - \beta^2 \tan^2 \epsilon}$
K_a	wing-angle ratio $\left(\frac{\alpha_a}{\alpha} \right)$
K_{aC}	wing-body-combination-angle ratio $\left(\frac{\alpha_a}{\alpha} \right)$
L	lift force, lb
M	free-stream Mach number
P	static-pressure coefficient, ratio of difference between local and free-stream static pressures to free-stream dynamic pressure
q	free-stream dynamic pressure, lb/sq in.
R	Reynolds number

s	wing semispan, in.
S	total wing-plan-form area as extended in figure 1 ($S = c_r s$), sq in.
t	maximum wing thickness, in.
α	angle of attack in radians unless otherwise specified
α_a	rearward inclination of force due to angle of attack, radians
β	$\sqrt{M^2 - 1}$
γ	ratio of specific heat at constant pressure to specific heat at constant volume
ϵ	wing semiapex angle, deg
η	correction for three-dimensional effects on body
λ	modification factor to account for finite-wing aspect ratios
Λ_0	sweep angle of wing leading edge, deg
$\Lambda_{\frac{1}{2}}$	sweep angle of wing midchord line, deg
τ	thickness ratio $\left(\frac{t}{c_r}\right)$

Subscripts

B	body alone
C	wing-body combination
C-N	combination minus nose
N	body nose
W	wing alone (exposed half wings joined together)
WB	effect of exposed half wings on body
BW	effect of body on exposed half wings (includes effect of separating half wings)

EXPERIMENTAL CONSIDERATIONS

The tests were performed in the Ames 1- by 3-foot supersonic wind tunnel No. 1. The apparatus and procedure are described in detail in reference 1. The models were tested through a nominal angle-of-attack range of $\pm 5.5^\circ$ at Mach numbers of 1.50 and 2.02 and at a constant Reynolds number of 0.5 million per inch.

Models

The body (fig. 1) had a fineness ratio of 7.33, a conical nose with a semiapex angle of 15° , and an ogival transition section fairing into a cylindrical afterbody. Tests were made with the body in a smooth condition and with transition fixed by a 0.003-inch-diameter wire at 5 percent of the body length from the nose. Calculations indicated that the drag of the wire was negligible compared to that of the body. The geometrical properties and designations of the six wing models used in the investigation are summarized in table I. The wings had symmetrical double-wedge airfoil sections in the streamwise direction with a maximum thickness of 8 percent at the midchord. The wings were located along the cylindrical part of the body for all the wing-body combinations. A wing and a wing-body combination mounted in the wind tunnel are shown in figure 2.

In order to estimate the support interference occurring in the wing-alone tests, pressures were measured inside the shroud shown in figure 2. The pressure 2 inches behind the opening in the shroud was the same as that at the far end of the balance for all test conditions. If any pressure difference across the wing support existed, it was confined to a small region near the tip of the shroud, and a conservative estimate for the effect upon the wing of lowest aspect ratio indicated a possible error in lift-curve slope of 0.5 percent. For wings of greater aspect ratio, this error was, of course, much less. The effect of the thin, beveled sting in modifying the lift of the wing was negligible; the effect on the drag was to cause a measurement that was about 1 percent too large. The data were not corrected for this small error.

Corrections to Experimental Results

The experimental data have been corrected for nonuniform flow conditions in the tunnel test section. The longitudinal pressure gradients in the empty tunnel were assumed to act unchanged on the model in the tunnel, and it was found, in general, that the corrections to drag were small but not negligible. The maximum correction to drag coefficient for all configurations at both Mach numbers was 13 percent of the measured drag coefficient.

Precision

The precision of the data has been evaluated by the method outlined in reference 3 and in reference 4. This method includes an estimate of the precision of each measurement and the resulting uncertainty in each measurement. It also includes an estimate of the uncertainty involved in the corrections to the data. The total uncertainty in the results is taken as the square root of the sum of the squares of the individual uncertainties.

The following table lists the total uncertainty for all configurations at both Mach numbers:

Quantity ¹	Uncertainty					
	Body		Wings		Combinations	
	$C_L = 0$	$C_{L_{max}}^2$	$C_L = 0$	$C_{L_{max}}$	$C_L = 0$	$C_{L_{max}}$
M	±0.02	±0.02	±0.02	±0.02	±0.02	±0.02
C_D	±0.0067	±0.0083	±0.0005	±0.0014	±0.0012	±0.0017
C_L	±0.009	±0.009	±0.009	±0.009	±0.009	±0.009

¹The values for the uncertainty in C_L were taken from reference 1.

²The quantity $C_{L_{max}}$ is the maximum C_L reached in the tests.

THEORETICAL CONSIDERATIONS

Body

Minimum drag.— The minimum drag of a pointed body of revolution consists of pressure and skin-friction drag. The pressures on the nose of the cylindrical body of the present investigation were calculated by the method of characteristics (reference 5) and integrated to give the minimum pressure drag:

$$C_{Dp} = 2 \int_0^1 P \left(\frac{a}{a_{max}} \right) d \left(\frac{a}{a_{max}} \right) \quad (1)$$

No attempt was made to predict the base drag because the measured drag data were adjusted to correspond to a base pressure equal to the static pressure of the free stream. The friction drag was calculated using the incompressible, flat-plate, laminar skin-friction law of Blasius

$$C_F = \frac{1.328}{\sqrt{R}} \quad (2)$$

because the effects of assuming a flat plate (reference 6) and the effects of compressibility on laminar skin friction (reference 7) were theoretically found to be small in the present tests. For the same body with a 0.003-inch-diameter transition wire on the nose, von Kármán's flat-plate, compressible, turbulent, skin-friction formula (reference 8)

$$\frac{0.242}{\sqrt{C_F}} \left(1 + \frac{\gamma - 1}{2} M^2\right)^{-\frac{1}{2}} = \log_{10}(R C_F) - \frac{1}{2} \log_{10}\left(1 + \frac{\gamma - 1}{2} M^2\right) \quad (3)$$

was used.

Drag rise.— The drag rise of the body with angle of attack is given by the slender-body theory of Ward (reference 9) as

$$\Delta C_D = \frac{1}{2} C_L \alpha = \alpha^2 \quad (4)$$

If the effect of cross-flow separation is taken into account, the theory of Allen and Perkins (reference 10) gives the drag rise as

$$\Delta C_D = \alpha^2 + \eta c_{d_c} \frac{A_p}{x_{\max}^2} \alpha^3 \quad (5)$$

For a cylinder with the same fineness ratio as the present body, reference 10 gives $\eta=0.65$. This value, together with $c_{d_c}=1.2$, has been used with equation (5) in determining the theoretical drag rise of the body.

Wings

Minimum drag.— The minimum pressure drag coefficients of the wings were computed from the linear theory of Puckett (reference 11). The friction drag coefficient was assumed to be independent of angle of attack and was estimated from the formula (reference 4)

$$C_{D_f} = 2 \left[C_{f_{\text{turb}}} - \frac{S_{\text{lam}}}{S} (C'_{f_{\text{turb}}} - C'_{f_{\text{lam}}}) \right] \quad (6)$$

which assumes that the profile of the turbulent region was the same as if the boundary layer had been turbulent up to the transition point. The extent of laminar and turbulent boundary layer on the wings was estimated from the theoretical chordwise pressure distribution. The laminar area was assumed to extend over the region of favorable gradients from the wing leading edge to the ridge line for wings with

subsonic ridge lines and from the leading edge to the Mach line emanating from the apex of the ridge lines for the wings with supersonic ridge lines. The laminar and turbulent friction coefficients were calculated using equations (2) and (3), respectively.

Drag rise.- The wing drag rise with angle of attack was calculated using the wing drag-rise factor (reference 4)

$$\frac{\Delta C_D}{C_L^2} = \frac{K_a}{(dC_L/d\alpha)} \quad (7)$$

where K_a defines the rearward inclination of the resultant force as a fraction of the angle of attack. The theoretical value of K_a depends on the wing plan form and the Mach number and is given by

$$K_a = 1 - \frac{\sqrt{1 - \beta^2 \tan^2 \epsilon}}{2 E} \quad (8)$$

For triangular wings with supersonic leading edges ($\beta \tan \epsilon > 1$), K_a is equal to one. The drag-rise factor is then

$$\frac{\Delta C_D}{C_L^2} = \frac{1}{(dC_L/d\alpha)} \quad (9)$$

Wing-Body Combinations

Minimum drag.- In order to predict the minimum drag of a wing-body combination, the interference effects of the wing on the body and of the body on the wing as well as the drag of the body and wings alone must be known. The pressures on the wing in the presence of the body were calculated by the method of Nielsen and Matteson (reference 2). These calculations indicated that for the present wing-body combinations the interference pressure drag would not be large if the wing alone were defined as the exposed half wings brought together rather than as the total wing which was utilized for lift and pitching-moment interference in reference 1. Since the drag of the body and wings alone is much more amenable to calculation than the interference drag, it is desirable to define the interference in such a manner that it becomes a small correction to the body and wing-alone drag. Thus, the minimum drag of the wing-body combinations was considered to consist of the sum of the drag of the body alone, the drag of the exposed wings joined together, the interference drag on the half wings resulting from separating the half wings and placing them in the presence of the body, and

the interference drag on the body resulting from placing the body in the presence of the exposed wings. These drag components were calculated as follows: (a) The drag of the body alone was calculated as discussed previously, with the boundary layer assumed to be laminar. (b) The drag of the exposed wings joined together was calculated in the same manner as that of the total wing alone. Inasmuch as the wing aspect ratio was the same, the wing pressure-drag coefficient was the same as that of the total wing alone. However, the friction-drag coefficient was greater than that of the total wing because the Reynolds number was less for the exposed wing. (c) The interference pressure drag on the exposed wings due to the body, which includes the effect of separating the half wings and placing them in the presence of the body, was calculated by the method of reference 2. This procedure does not include the effect of the body nose on the drag of the exposed wings. Calculations indicate that this effect was negligible. Although the maximum interference pressure drag was 24 percent of the pressure drag of the exposed wings joined together (for W_1B at $M=1.50$), with the wing alone as defined above it was never greater than 2 percent of the total drag of any of the wing-body combinations. It was assumed that the interference friction drag on the wings was negligible. This assumption was substantiated by experiments to be described later. (d) The interference pressure drag of the wings on the body at zero angle of attack was zero because the wings were located along the cylindrical part of the body. It was assumed, and was also substantiated by experiments to be described later, that the interference friction drag of the wings on the body was a result of the wing shock wave causing transition on the body at the intersection of the wing-leading-edge shock wave and the body. The interference friction drag of the wing on the body was then calculated as the difference between the friction drag on the body assuming part laminar, part turbulent skin friction, and the friction drag on the body with the boundary layer completely laminar.

Drag rise.— The drag rise with angle of attack of the wing-body combinations was calculated as the sum of the drag rise of the body nose and that of the winged part of the combinations

$$\Delta D_C = \Delta D_N + \Delta D_{C-N} \quad (10)$$

where the winged part of the combination consisted of the exposed wings and the part of the body included between them.

Equation (4), which does not include effects of cross-flow separation, was used to calculate the drag rise of the body nose. There is no inconsistency in calculating the drag rise of the body alone on the basis of equation (5) and that of the body of the wing-body combinations on the basis of equation (4) inasmuch as the effect of cross-flow

separation on the body alone is small (theoretically a maximum of 2 percent of the drag coefficient of W_1B at $\alpha=5.5^\circ$) and is less for the body of the wing-body combinations. This reduction, relative to that of the body alone, occurs because in the region of the wing the flow is directed along the wing; behind the wing, the downwash reduces the cross flow.

In the calculation of the drag rise of the winged portion of the combination, an assumption was made that the same wing leading-edge suction factor K_a can be applied as for the wing alone. This is valid as the wing aspect ratio approaches zero since K_a is equal to 0.5 for both a wing and a wing-body combination for this limiting case. The assumption is also valid as the wing span becomes very large relative to the body diameter since the effect of the body then becomes negligible. The wing-body-combination drag due to lift is then

$$\Delta D_C = \frac{1}{2} \alpha L_N + K_a \alpha L_{C-N} \quad (11)$$

Spreiter has shown (reference 12) that, if the wing-body combination is slender, the lift coefficient of the winged part of the combination is

$$C_{L_{C-N}} = 2\pi\alpha \left(1 - \frac{a_{\max}^2}{s^2} \right)^2 \tan \epsilon \quad (12)$$

It was shown experimentally (reference 1) that equation (12) is applicable to combinations with high aspect-ratio triangular wings similar to those of the present tests when the equation is modified by the factor λ . For triangular wings, the factor λ is defined as follows:

$$\left. \begin{aligned} \lambda &= \frac{1}{E} & \beta \tan \epsilon &\leq 1 \\ \lambda &= \frac{2}{\pi\beta \tan \epsilon} & \beta \tan \epsilon &\geq 1 \end{aligned} \right\} \quad (13)$$

The lift coefficient of the winged part of the combination is then

$$C_{L_{C-N}} = 2\pi\alpha \lambda \left(1 - \frac{a_{\max}^2}{s^2} \right)^2 \tan \epsilon \quad (14)$$

By combining equations (4) and (14), the drag due to lift of the combination, in coefficient form, is

$$\Delta C_{DC} = 2\pi\alpha^2 \left[\frac{1}{2} \left(\frac{a_{max}}{s} \right)^2 + K_a \lambda \left(1 - \frac{a_{max}^2}{s^2} \right)^2 \right] \tan \epsilon \quad (15)$$

The lift coefficient of the complete wing-body combination is (reference 1)

$$C_{LC} = \frac{L_N + L_{C-N}}{qS} = 2\pi\alpha \left[\left(\frac{a_{max}}{s} \right)^2 + \lambda \left(1 - \frac{a_{max}^2}{s^2} \right)^2 \right] \tan \epsilon \quad (16)$$

Thus, the drag-rise factor is

$$\frac{\Delta C_{DC}}{C_{LC}^2} = \frac{1}{\left(\frac{dC_{LC}}{d\alpha} \right)} \left[\frac{\frac{1}{2} \left(\frac{a_{max}}{s} \right)^2 + K_a \lambda \left(1 - \frac{a_{max}^2}{s^2} \right)^2}{\left(\frac{a_{max}}{s} \right)^2 + \lambda \left(1 - \frac{a_{max}^2}{s^2} \right)^2} \right] \quad (17)$$

For the cases in which no wing leading-edge suction is to be expected (supersonic leading edges) K_a is equal to one.

RESULTS AND DISCUSSION

In order to isolate experimentally the total interference ratio $\frac{D_{WB} + D_{BW}}{D_B + D_W}$, the characteristics of the body alone, the wings alone, and the combinations must be measured. The results of the tests to determine these characteristics are discussed individually and are presented in the form of drag coefficients as a function of the lift coefficients in figures 3 to 5 for the body, wings, and combinations, respectively. The results are summarized in table II. From these data, the total interference ratio was determined. It must be pointed out that the experimental results for the wing alone pertain to the total wing. The term D_W in the interference ratio was obtained by applying the experimental drag coefficient of the total wing to the exposed wing area. This introduces a skin-friction error in D_W but the resulting error in the drag interference ratio was negligible.

Body

The experimental and calculated drag polars for the body with and without a 0.003-inch-diameter wire at 5 percent of the body length from

the nose to fix transition are presented in figure 3. It can be seen that the experimental minimum drag coefficients for the body with and without the wire were in good agreement with the calculated values that included either completely laminar or completely turbulent skin-friction coefficients. However, the theoretical drag rise for the body without the wire was much less than that measured experimentally. This difference can be attributed to the fact that no change in skin friction with angle of attack was assumed in the theory. The data indicate that this assumption was not valid and it is believed that the skin friction increased with angle of attack, probably a result of forward movement of the transition point. For the body with transition fixed, little change in skin friction was indicated and the experimental and theoretical drag-rise values were in fair agreement.

Wings

Minimum drag.- The minimum drag coefficients of the wings alone are presented in figure 6 as a function of $\beta \tan \epsilon$. For values of $\beta \tan \epsilon$ greater than 0.4, the calculated minimum drag coefficients were larger than those measured experimentally. It was shown in reference 1 that higher-order effects had a decided influence on the lift coefficients of 8-percent-thick triangular wings. Thus for the present wings, higher-order effects on the drag coefficients and differences between theoretical results calculated on the basis of the linear theory and experimental results are to be expected. For values of $\beta \tan \epsilon$ less than 0.4, the flow over the wings was also expected to differ from that predicted by the linear theory because of the vortex-type flow known to exist over these low-aspect-ratio wings (reference 13). Thus, the good agreement between the experimental and theoretical minimum drag coefficients in this range of values of $\beta \tan \epsilon$ was possibly a result of compensating factors.

Drag rise.- The wing-alone drag-rise results are presented in terms of the drag-rise factor $\Delta C_D/C_L^2$ in figure 7(a), and in terms of the relative inclination of the change in the resultant force due to lift as a fraction of the angle of attack, K_a , in figure 7(b). The experimental values of $\Delta C_D/C_L^2$ were determined by evaluating the slopes of straight lines faired through plots of ΔC_D versus C_L^2 . The experimental values of K_a were determined by the product of $dC_L/d\alpha$ and $\Delta C_D/C_L^2$. Comparison between theory and experiment would seem to indicate that, for the wings with subsonic leading edges, nearly all the predicted leading-edge suction was realized. However, this conclusion cannot be made because other factors such as a decrease in skin friction with an increase in angle of attack, or forward movement of the shock wave at the trailing edge (reference 14) of the upper surface of the wing, would have the same effect on the drag as an

attainment of leading-edge suction. These same factors could also account for the fact that K_a for the wings with supersonic leading edges was less than the theoretical value of unity.

Wing-Body Combinations

Minimum drag. - The minimum drag coefficients of the wing-body combinations are summarized in figure 8. It can be seen that the experimental and theoretical minimum drag coefficients were in good agreement - better agreement than that for the wings alone. This fact can be accounted for by the large percentage of body drag in the drag of the combinations (theoretically 94 percent for the lowest and 51 percent for the highest aspect ratio). The body pressure drag was analyzed by the method of characteristics, whereas the pressure drag of the wings alone was calculated by linear theory. The greater accuracy in the predicted body drag compared to that of the wing is evident in the results.

The validity of the assumptions made in regard to the type of boundary-layer flow on the wing-body combinations at zero angle of attack is shown by the sketches in figure 9 which were made from liquid-film studies. It can be seen that the proportion of laminar and turbulent boundary layer on the wing alone was essentially the same as that on the wing in the presence of the body. However, the presence of the wing caused transition on the body at the juncture with the wing leading-edge shock wave.

Drag rise. - The drag-rise characteristics of the wing-body combinations are presented in figure 10. It can be seen that the agreement was fair between the calculated values, which do not include leading-edge suction on the wings, and the experimental values. However, for the combinations with the lowest aspect-ratio wings, the calculated drag-rise factor $\Delta C_D/C_L^2$ and the relative inclination of the change in resultant force K_{aC} , which include leading-edge suction on the wings, were approximately 50 percent of the experimental values. This difference decreased for combinations with higher aspect-ratio wings. Thus, the discrepancy between the calculations and experiment was largest in the range of values of $\beta \tan \epsilon$ where the assumption of wing leading-edge suction should be applicable. Why leading-edge suction was effectively realized for the wings alone and not for the wing-body combinations is not clear.

Interference Effects

The components of the drag of a wing-body combination may be considered to be

$$D_C = D_W + D_B + D_{WB} + D_{BW}$$

where the wing alone is defined as the exposed half-wings joined together. The term D_{BW} is determined from the difference between the drag force on the wing alone and the drag force on the wing in the presence of the body. Thus D_{BW} is the effect of the body on the wing drag force. Similarly, D_{WB} is the effect of the wing on the body drag force. The total interference ratio is defined as

$$\frac{D_{WB} + D_{BW}}{D_B + D_W} = \frac{D_C}{D_B + D_W} - 1$$

Thus, the total drag-interference ratio may be obtained from the drag forces of the wings alone, body alone, and combinations.

Minimum drag.- The total drag-interference ratios at zero lift are shown as a function of the ratio of the wing semispan to the body radius and the wing aspect ratio in figure 11(a). Interference ratios are presented using both the measured body-alone results (laminar boundary layer) and also these results adjusted for the effect of the wing in causing transition on the body behind the juncture of the wing leading-edge shock wave and the body (see fig. 9). It can be seen that the interference would be unfavorable (the drag of the combinations being larger than the exposed wing-plus-body drag) if the drag of the body with a completely laminar boundary layer were used as the basis for the interference. The measured interference drag varied from 18 percent of the drag of the combination having the smallest wing relative to the body to 4 percent of the drag of the combination having the largest wing relative to the body. Agreement between the interference calculated by the method of reference 2, with friction effects taken into account, and the measured interference was good. The interference ratios were negligible with the body-alone boundary layer adjusted for the occurrence of transition behind the juncture of the wing leading-edge shock wave and the body. Thus, for configurations such as those tested, the interference drag force is caused principally by the effect of the wing on the boundary layer of the body. This would not necessarily be the case for wing-body combinations in which the wing was highly swept and contributed a major share of the drag of the combination. To accurately predict the minimum drag of such a wing-body combination it would be necessary to calculate the interference by some method such as that of reference 2. It is noted that, if the Reynolds number of the present tests had been such that natural transition occurred on the body in front of the wing-body juncture, the drag

interference at zero lift would have been negligible. This conclusion was borne out by tests on combination W_2B with transition fixed on the body nose. Therefore, it is evident that Reynolds number effects on drag interference can be large.

Angle of attack.- The total drag-interference ratios at an angle of attack of 5° are presented in figure 11(b). The interference ratios are presented only with the smooth body results because there was little difference in the drag coefficients of the smooth body and of the body with fixed transition at the lift coefficient for $\alpha=5^\circ$. (The lift coefficients at this angle of attack were taken from reference 1.) As for $\alpha=0^\circ$, the interference was unfavorable; but at $\alpha=5^\circ$, the interference remained approximately constant through the range of wing aspect ratios and values of s/a_{max} . The predicted and measured interference were in unexpectedly good agreement because the interference was presented in ratio form and because of compensating factors. The predicted drag coefficients of the body were less than the experimental values, but, for the combinations with low-aspect-ratio wings, this was balanced by the fact that the predicted drag coefficients of the combinations were also less than the experimental values. For the combinations with high-aspect-ratio wings, the high body-drag coefficients (relative to the calculated values) were offset by the low wing-drag coefficients.

CONCLUSIONS

In order to evaluate interference, the drag of a pointed cylindrical body, of six triangular wings having aspect ratios of 0.67 to 4.00, and of the wings and body in combination were investigated experimentally at Mach numbers of 1.50 and 2.02. The experimental measurements for the body, wings, and combinations, as well as the interference data, were compared with values predicted by available theories. The results support the following conclusions:

1. The minimum drag coefficients of the body alone, as calculated by the method of characteristics with laminar and turbulent skin-friction coefficients added for the body in a smooth condition and with fixed transition, were in good agreement with the corresponding experimental measurements. The drag rise with angle of attack, as calculated by the method of NACA Rep. 1048, 1951, was much lower than the experimental drag rise of the smooth body, but in fair agreement with that of the body with transition fixed. The evidence indicates that the transition point on the smooth body moved forward with increasing angle of attack, causing the skin friction to increase.

2. In general, the predicted minimum drag coefficients of the wings (which included an estimate of the skin friction) were greater than the experimental values.

3. The predicted minimum drag coefficients of the wing-body combinations were in good agreement with the experimental values. The better agreement for the combinations than for the wings alone was a result of the relatively greater accuracy in the calculation of the body drag which constitutes a large percentage of the combination drag.

4. Calculation of the pressures at zero angle of attack on the wings in the presence of the body by the method of NACA RM A9E19, 1949, indicated that the interference pressure drag would be small for the present wing-body combinations if the wing alone were defined as the exposed half-wings brought together. The experimental results indicated that the drag interference was principally the result of fixing transition on the body by adding a wing.

Ames Aeronautical Laboratory
National Advisory Committee for Aeronautics
Moffett Field, Calif., Mar. 27, 1951

REFERENCES

1. Nielsen, Jack N., Katzen, Elliott D., and Tang, Kenneth K.: Lift and Pitching-Moment Interference Between a Pointed Cylindrical Body and Triangular Wings of Various Aspect Ratios at Mach Numbers of 1.50 and 2.02. NACA TN 3795, 1956.
2. Nielsen, Jack N., and Matteson, Frederick H.: Calculative Method for Estimating the Interference Pressure Field at Zero Lift on a Symmetrical Swept-Back Wing Mounted on a Circular Cylindrical Body. NACA RM A9E19, 1949.
3. Michels, Walter C.: Advanced Electrical Measurements. Second ed., D. Van Nostrand Company, New York, 1943, p. 11.
4. Vincenti, Walter G., Nielsen, Jack N., and Matteson, Frederick H.: Investigation of Wing Characteristics at a Mach Number of 1.53. I - Triangular Wings of Aspect Ratio 2. NACA RM A7110, 1947.
5. Sauer, Robert: Introduction to Theoretical Gas Dynamics. J. W. Edwards, Ann Arbor, Michigan, 1947.
6. Mangler, W.: Compressible Boundary Layers on Bodies of Revolution. M.A.P. Völkenrode, Rep. and Trans. No. 47, Mar. 15, 1946.

7. Chapman, Dean R., and Rubesin, Morris: Temperature and Velocity Profiles in the Compressible Laminar Boundary Layer With Arbitrary Distribution of Surface Temperature. Jour. Aero. Sci., vol. 16, no. 9, Sept. 1949, pp. 547-565.
8. De Kármán, Th.: The Problems of Resistance in Compressible Fluids. Roma, Reale Accademia d'Italia, 1936. (GALCIT Pub. No. 75, 1936).
9. Ward, G. N.: Supersonic Flow Past Slender Pointed Bodies. Quart. Jour. Mech. and Appl. Math., vol. II, part I, March 1949, pp. 75-97.
10. Allen, H. Julian, and Perkins, Edward W.: A Study of Effects of Viscosity on Flow Over Slender Inclined Bodies of Revolution. NACA Rep. 1048, 1951.
11. Puckett, Allen E.: Supersonic Wave Drag of Thin Airfoils. Jour. Aero. Sci., vol. 13, no. 9, Sept. 1946, pp. 475-484.
12. Spreiter, John R.: The Aerodynamic Forces on Slender Plane- and Cruciform-Wing and Body Combinations. NACA Rep. 962, 1950. (Formerly NACA TN 1662)
13. Love, Eugene S.: Investigations at Supersonic Speeds of 22 Triangular Wings Representing Two airfoil Sections for Each of 11 Apex Angles. NACA Rep. 1238, 1955.
14. Ferri, Antonio: Elements of Aerodynamics of Supersonic Flows. The MacMillan Co., N. Y., 1949, pp. 143-144.

TABLE I.— SUMMARY OF GEOMETRICAL PROPERTIES OF WINGS







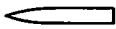












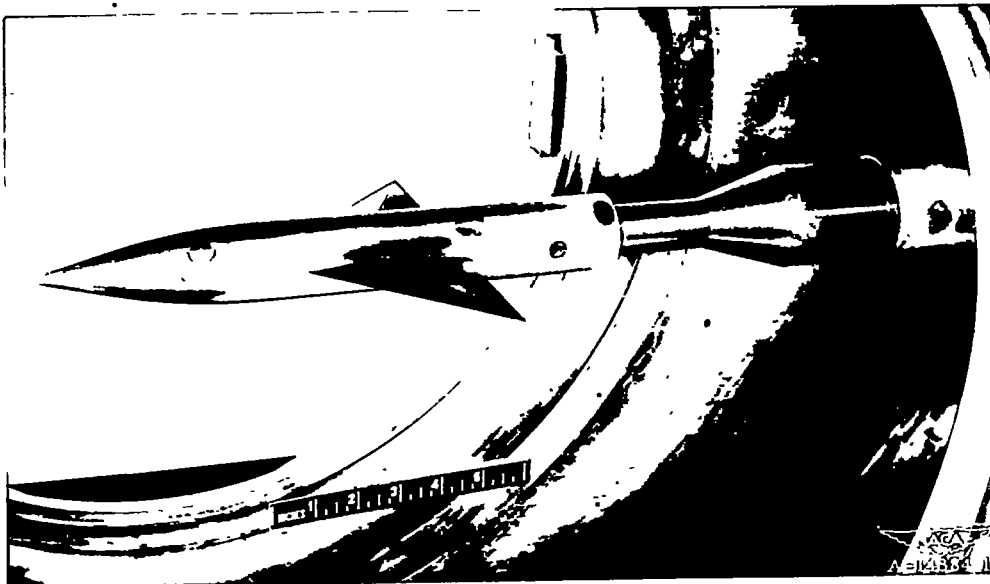
Wing	W_1	W_2	W_3	W_4	W_5	W_6
Sketch						
Λ_o (deg)	80.4	71.6	63.2	56.0	50.3	45.0
$\Lambda_{\frac{1}{2}}$ (deg)	71.4	56.2	44.7	36.6	31.0	26.6
s (in.)	1.25	1.75	2.25	2.76	3.24	3.74
\bar{c} (in.)	4.95	3.49	2.97	2.73	2.60	2.49
c_r (in.)	7.43	5.23	4.45	4.10	3.90	3.74
S (in. ²)	9.29	9.15	10.01	11.30	12.66	13.99
A	0.67	1.34	2.02	2.69	3.33	4.00
τ	.08	.08	.08	.08	.08	.08

TABLE II.-- SUMMARY OF RESULTS

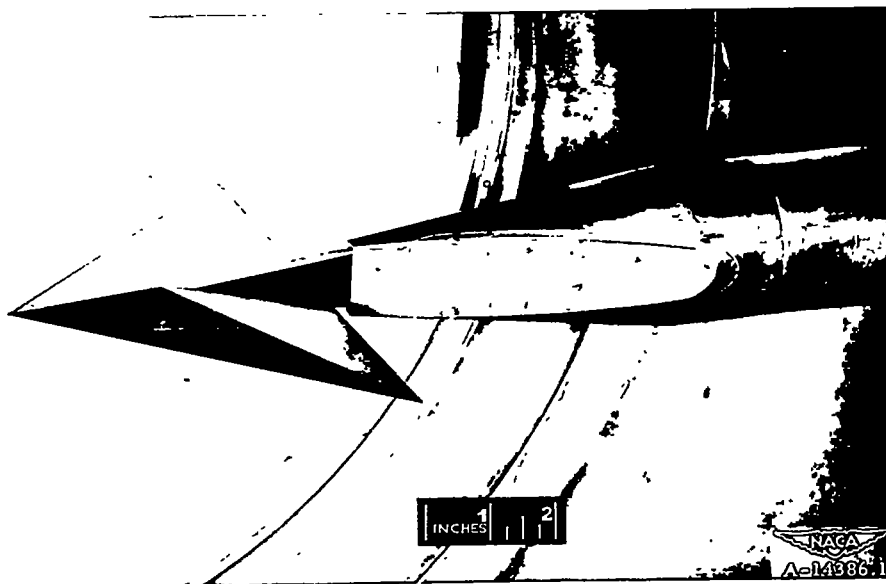
Configuration		Minimum drag		Drag rise			
Symbol	Sketch	$C_{D_{min}}$		$\Delta C_D/C_L^2$		K_a (for wings) or K_{ac} (for comb.)	
		M = 1.50	M = 2.02	M = 1.50	M = 2.02	M = 1.50	M = 2.02
B		0.145 (.140)	0.138 (.133)	— —	— —	— —	— —
W ₁		.0114 (.0117)	.0118 (.0110)	0.58 (.53)	0.58 (.59)	0.63 (.53)	0.62 (.56)
W ₂		.0185 (.0183)	.0160 (.0192)	.34 (.32)	.40 (.41)	.59 (.59)	.62 (.68)
W ₃		.0236 (.0286)	.0173 (.0198)	.34 (.27)	.40 (.39)	.76 (.67)	.80 (.84)
W ₄		.0252 (.0290)	.0172 (.0203)	.31 (.25)	.41 (.44)	.80 (.76)	.93 (1.00)
W ₅		.0261 (.0301)	.0185 (.0194)	.28 (.25)	.36 (.44)	.82 (.88)	.88 (1.00)
W ₆		.0270 (.0308)	.0188 (.0189)	.29 (.28)	.39 (.44)	.91 (1.00)	.94 (1.00)
W ₁ B		.0342 (.0336)	.0332 (.0308)	1.03 (.65)	1.18 (.69)	.95 (.52)	1.10 (.53)
W ₂ B		.0402 (.0377)	.0351 (.0357)	.51 (.35)	.65 (.43)	.87 (.57)	1.03 (.63)
W ₃ B		.0413 (.0417)	.0354 (.0359)	.38 (.27)	.52 (.38)	.88 (.64)	1.11 (.78)
W ₄ B		.0405 (.0410)	.0339 (.0348)	.33 (.25)	.47 (.41)	.90 (.73)	1.11 (.93)
W ₅ B		.0395 (.0405)	.0340 (.0327)	.30 (.25)	.42 (.41)	.90 (.85)	1.08 (.94)
W ₆ B		.0388 (.0407)	.0307 (.0315)	.27 (.27)	.40 (.40)	.89 (.96)	1.05 (.95)

Notes: 1. In each case the experimental value is given first and the corresponding theoretical value indicated in parenthesis directly below.

2. The theoretical drag rise values include full leading-edge suction on the wings and a wing leading-edge suction factor on the winged part of the combinations.



(a) Wing-body combination.



(b) Wing alone.

Figure 2.— Wing and wing-body combination mounted in tunnel.

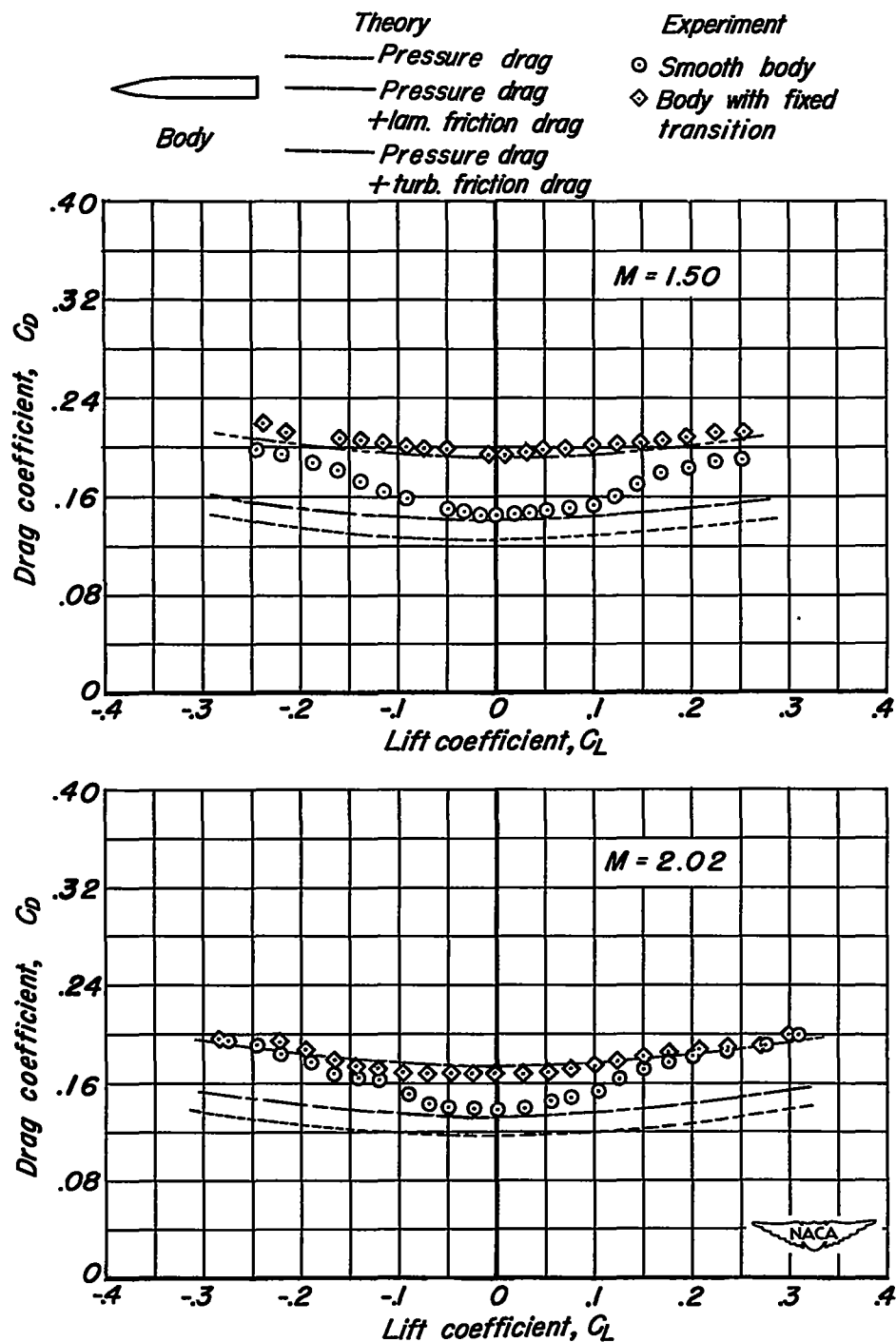
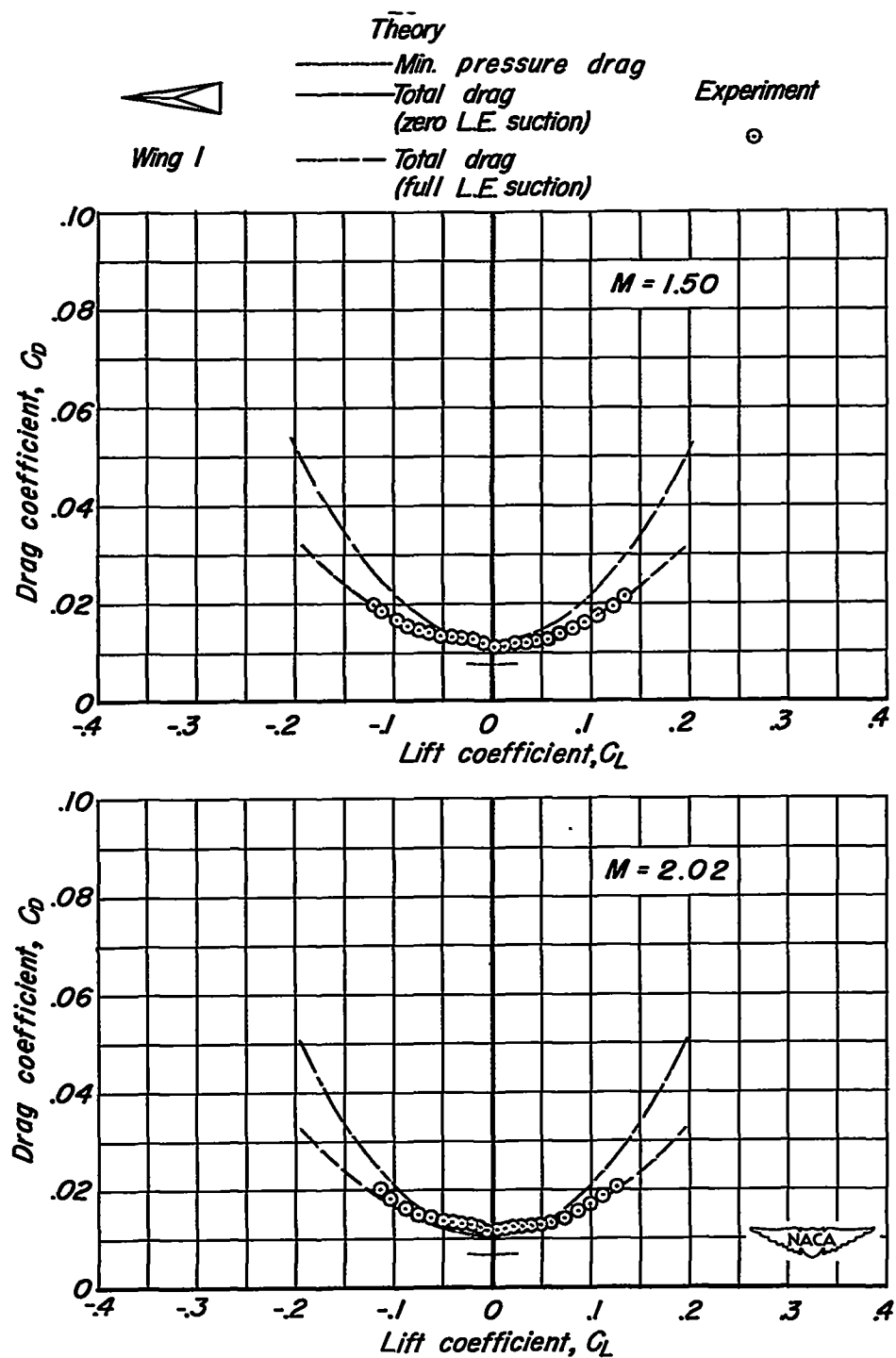
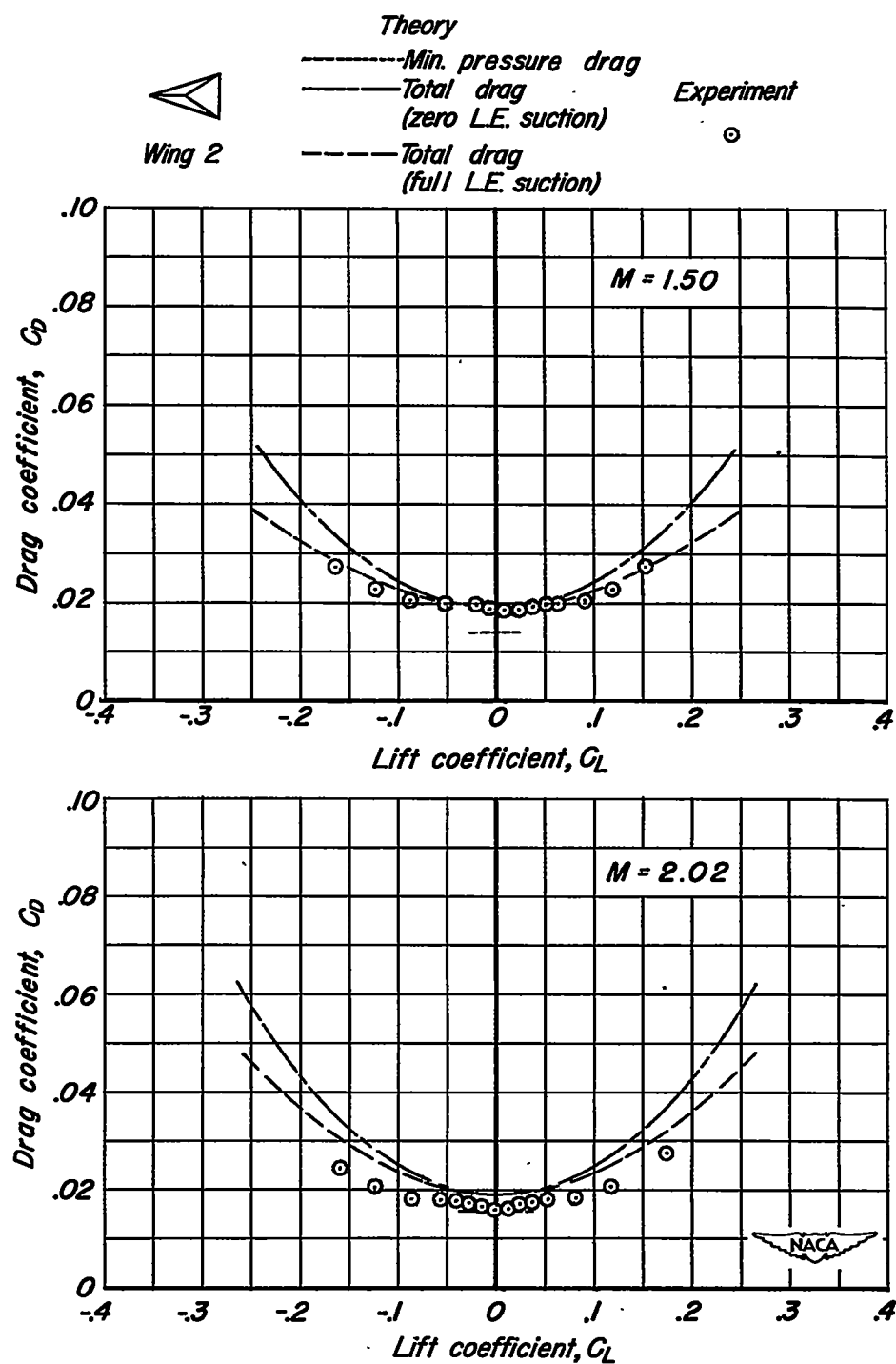


Figure 3. — Drag coefficient of body.



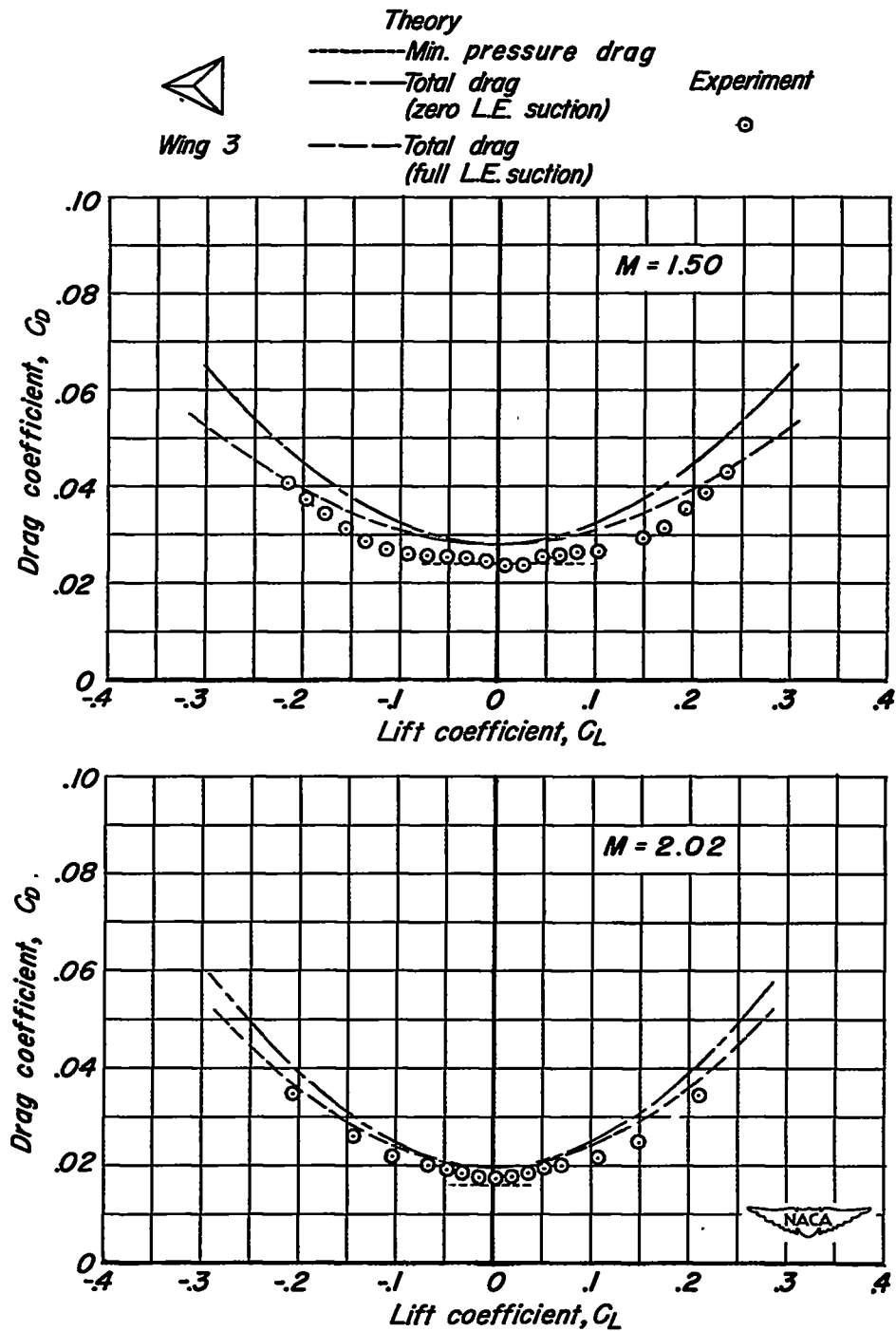
(a) Wing I.

Figure 4. — Drag coefficient of wings.



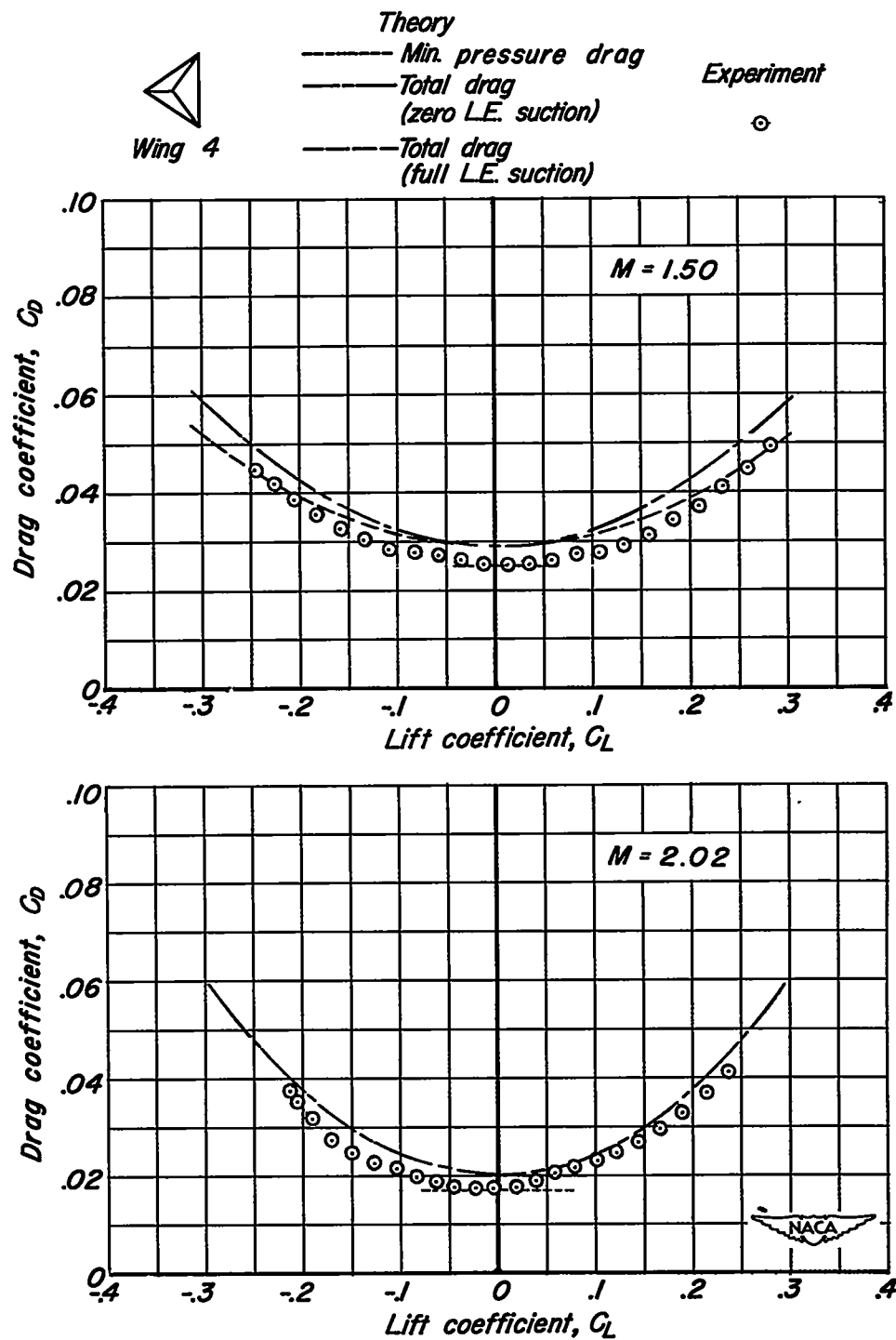
(b) Wing 2.

Figure 4. — Continued.



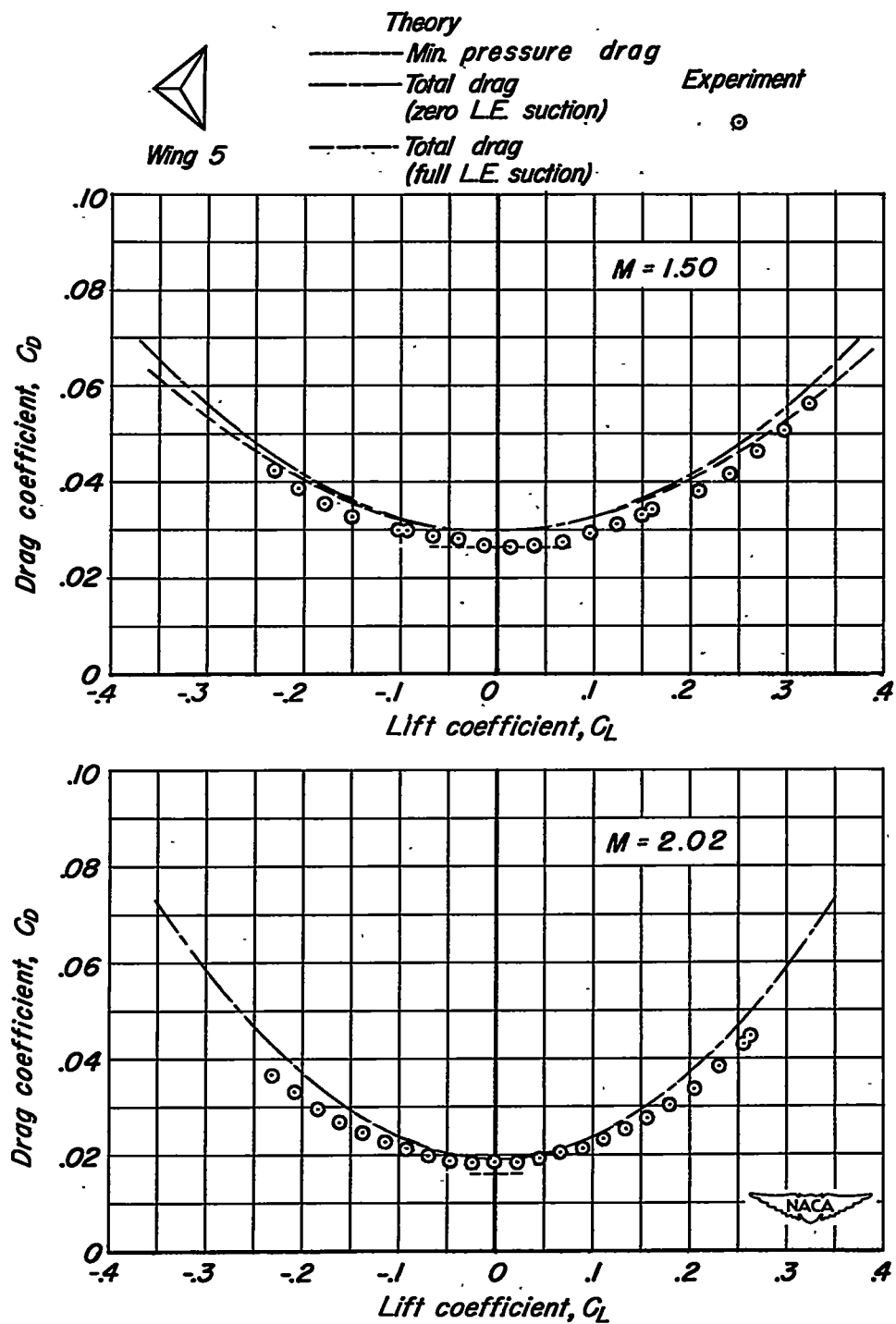
(c) Wing 3.

Figure 4. — Continued



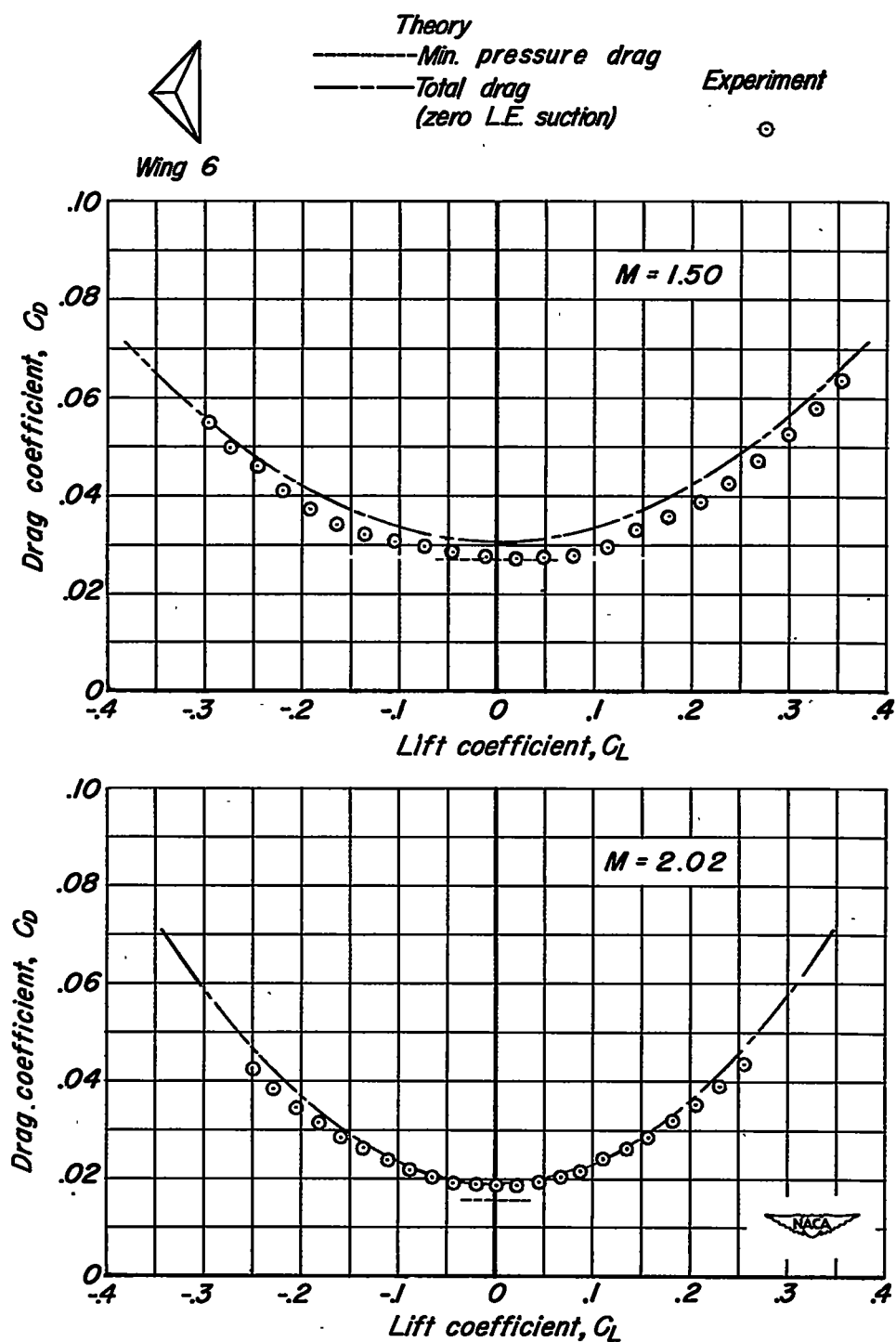
(d) Wing 4.

Figure 4.— Continued.



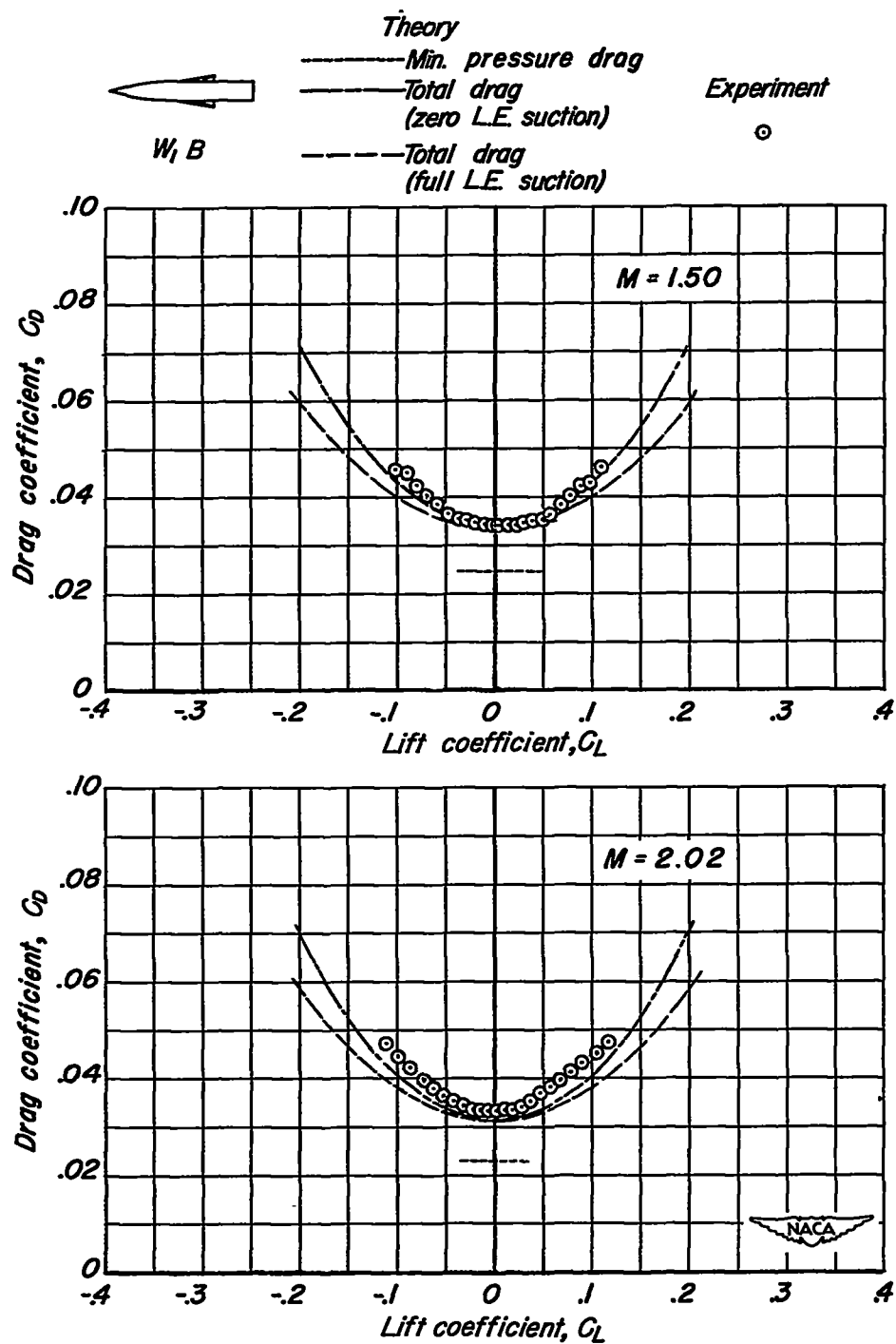
(e) Wing 5.

Figure 4. — Continued.



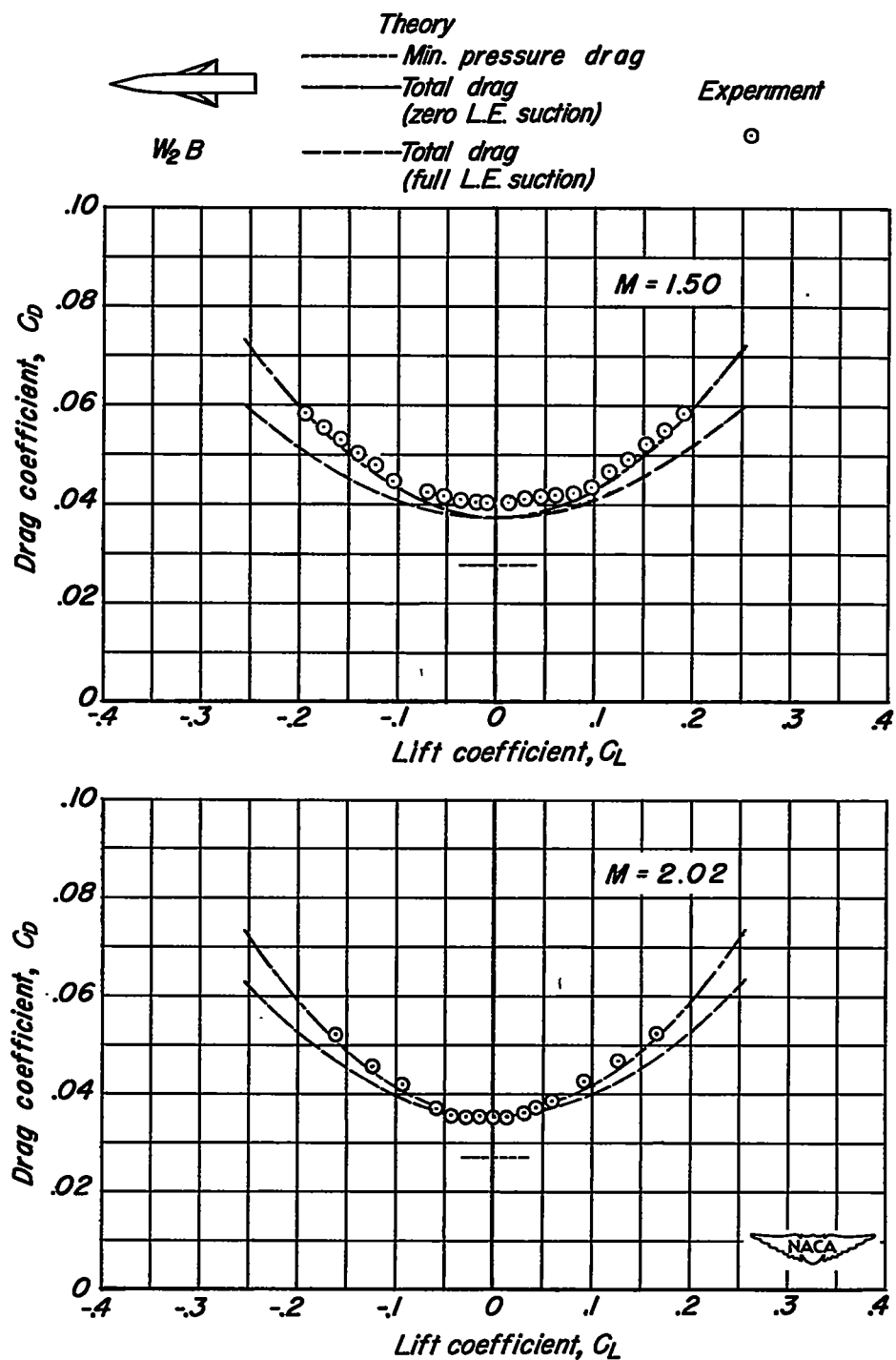
(f) Wing 6.

Figure 4. - Concluded.



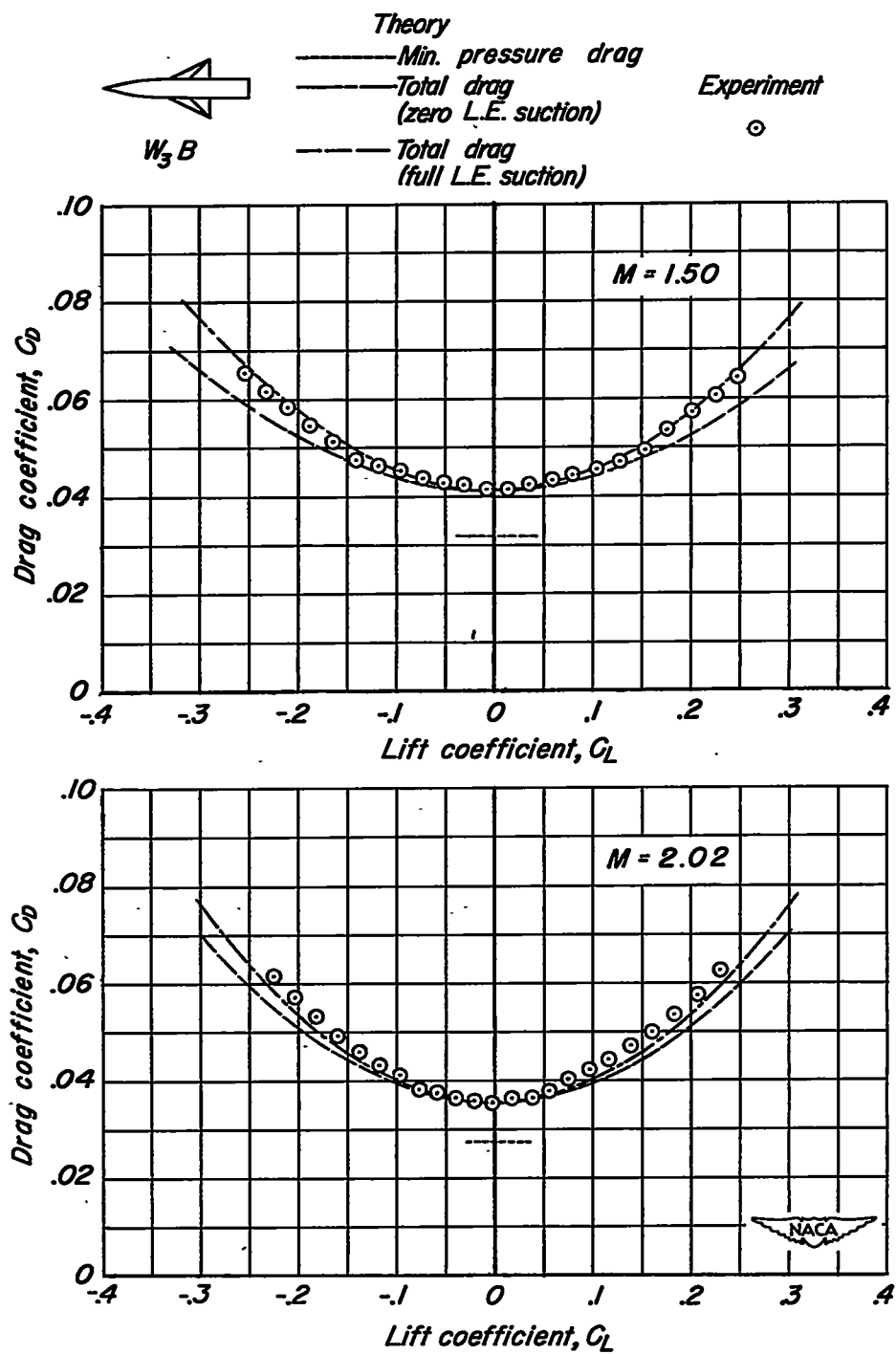
(a) Combination W_1B .

Figure 5. — Drag coefficient of combinations.



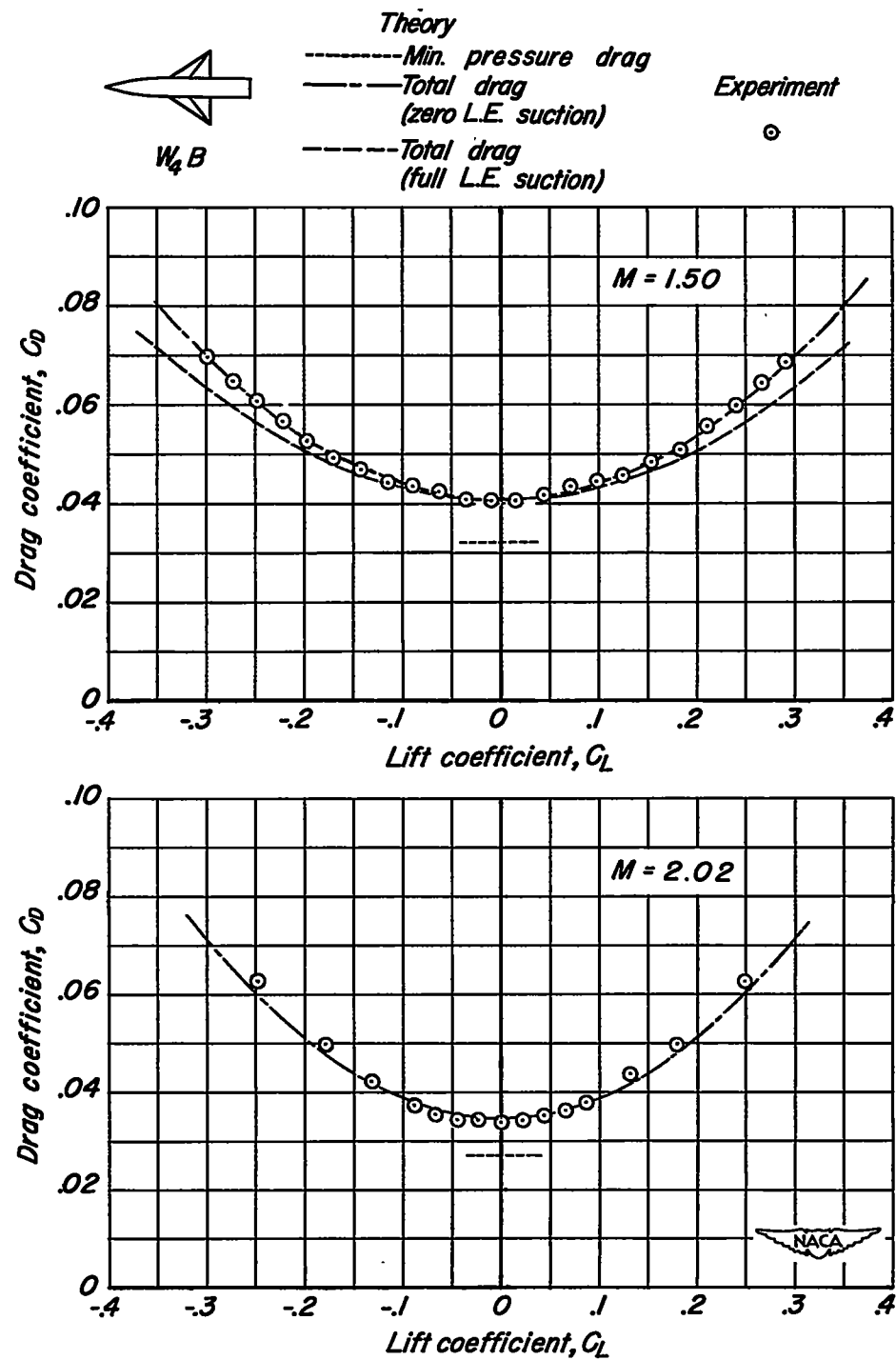
(b) Combination $W_2 B$.

Figure 5 — Continued.



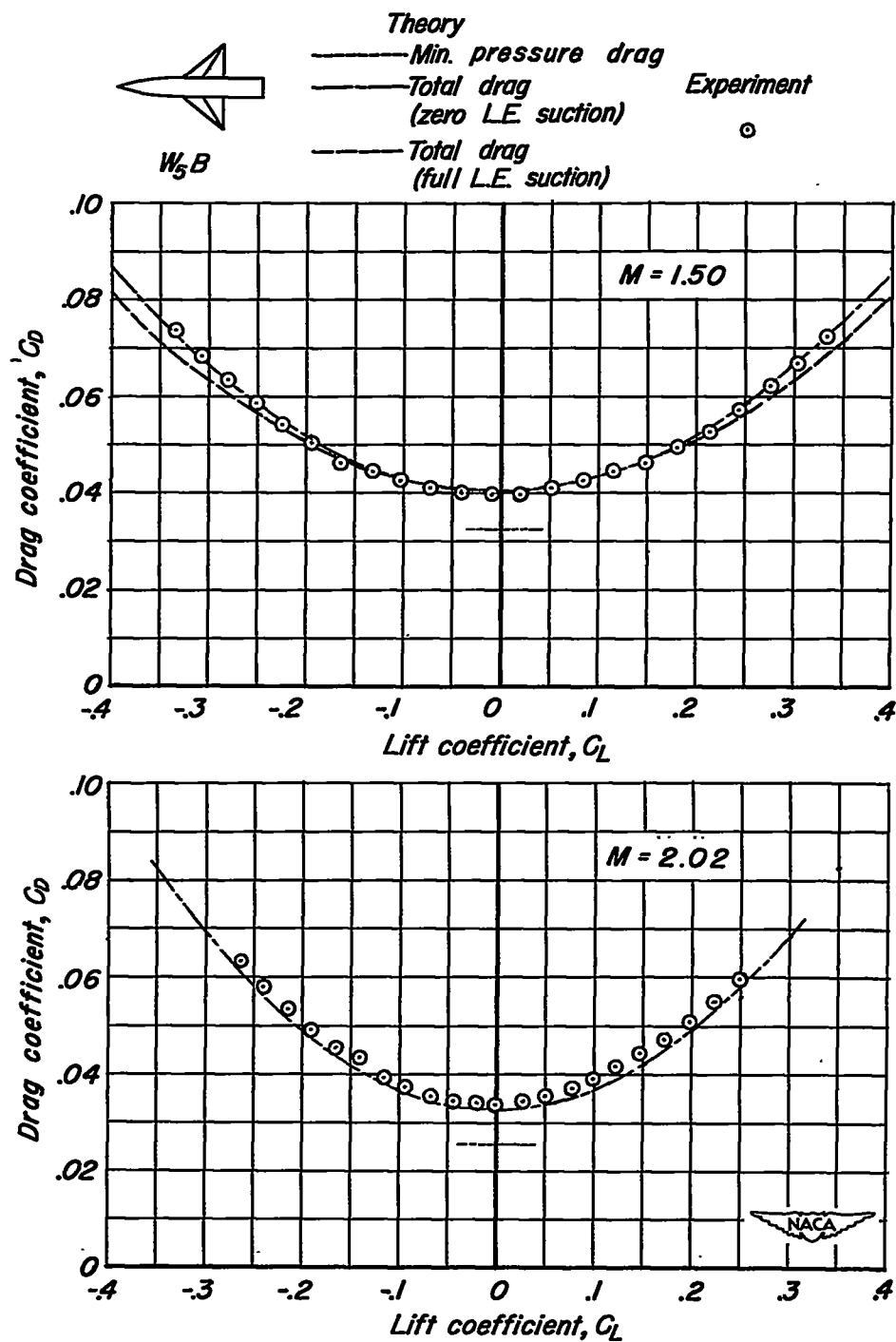
(c) Combination W_3B .

Figure 5 — Continued.



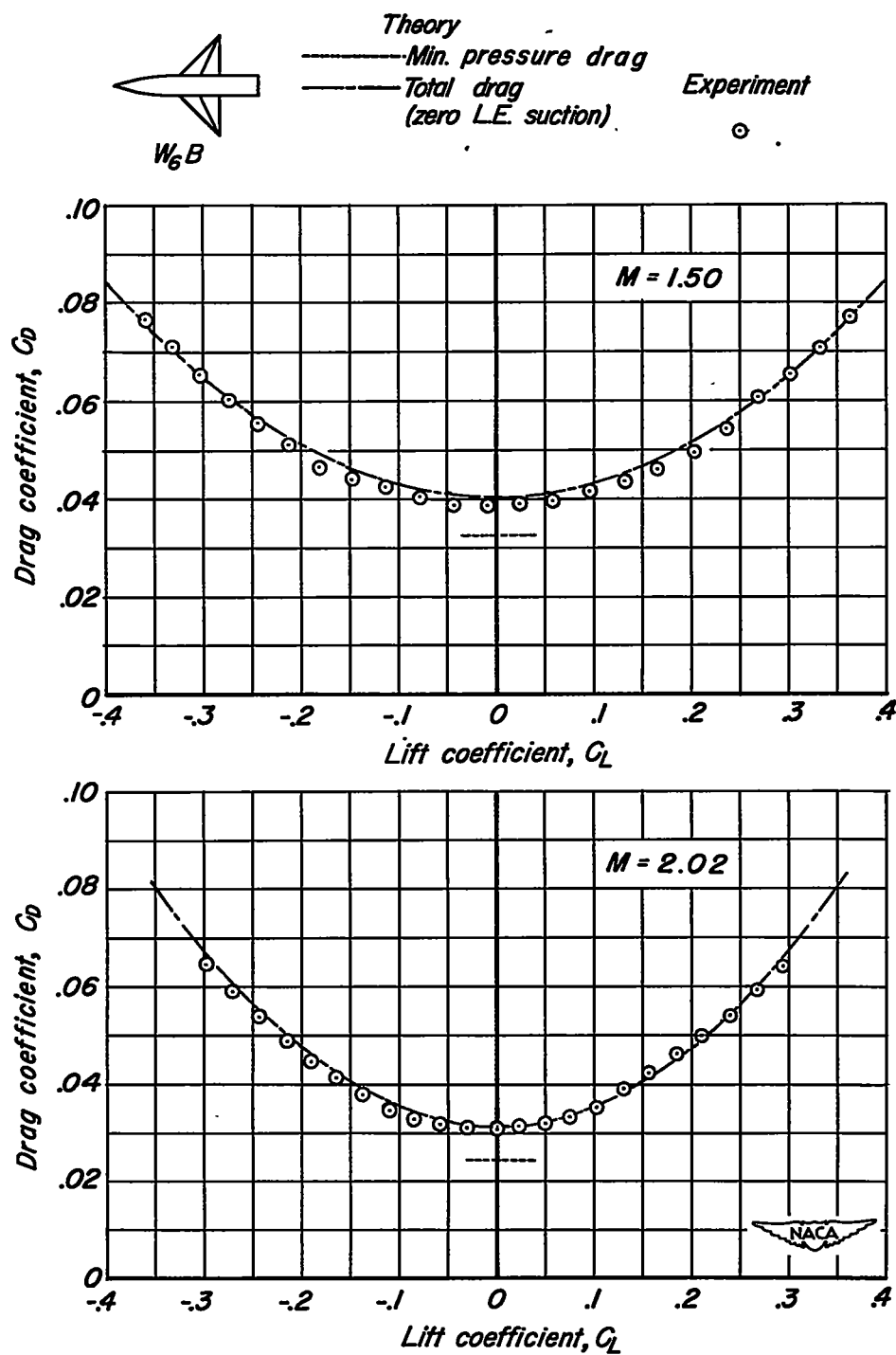
(d) Combination $W_4 B$.

Figure 5 — Continued.



(e) Combination W_5B .

Figure 5. — Continued.



(f) Combination W_6B .

Figure 5. — Concluded.

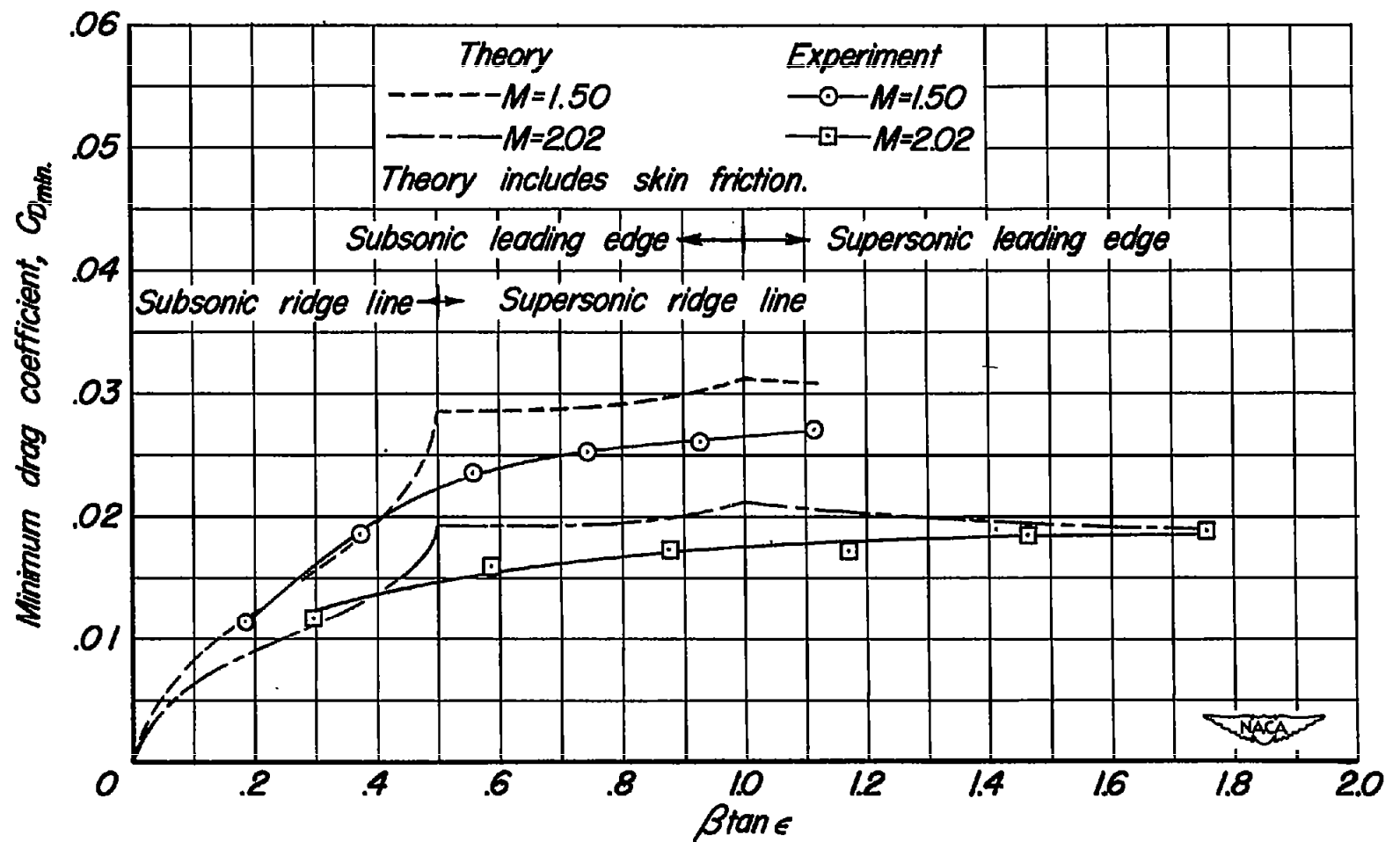


Figure 6.—Minimum drag coefficient of wings.

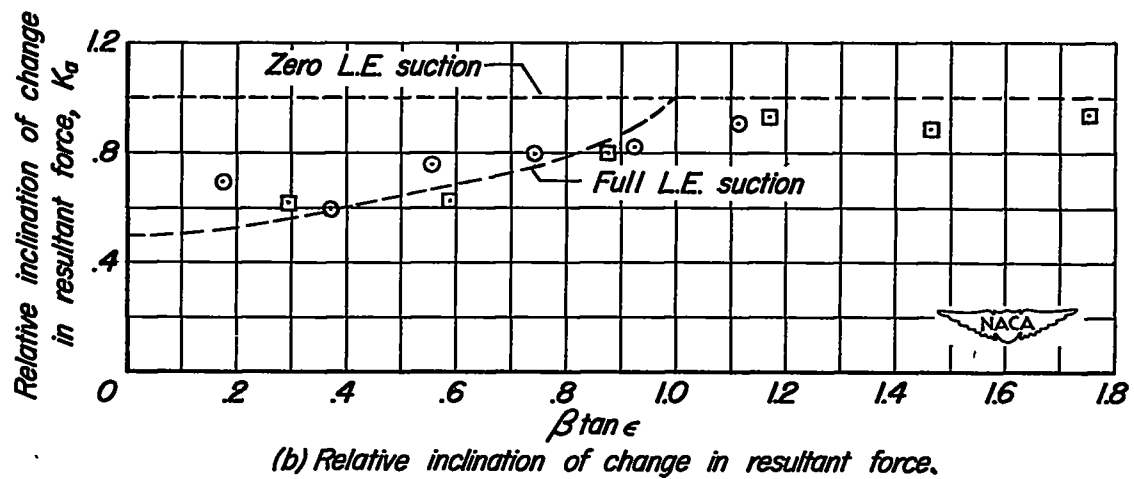
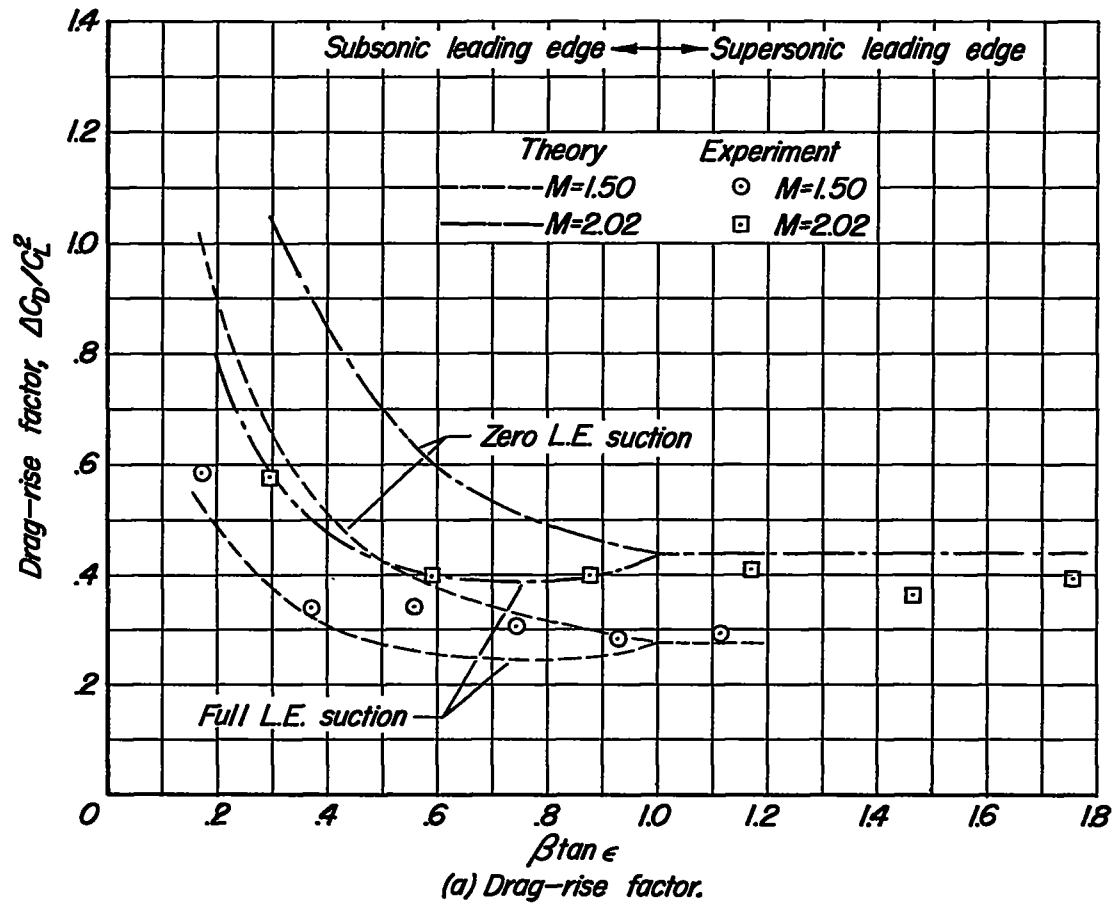


Figure 7.—Drag-rise characteristics of wings.

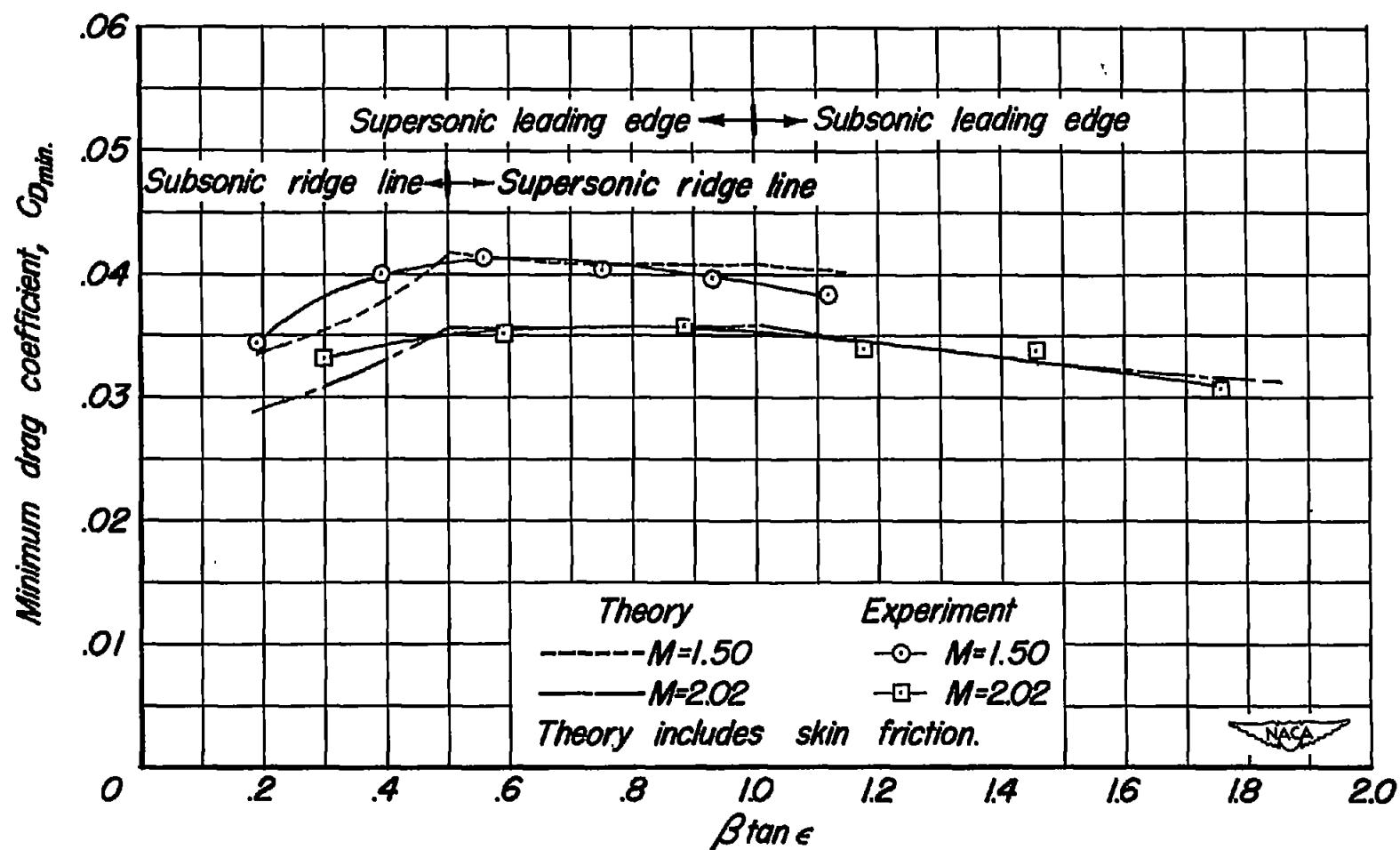


Figure 8.—Minimum drag coefficients of wing-body combinations.

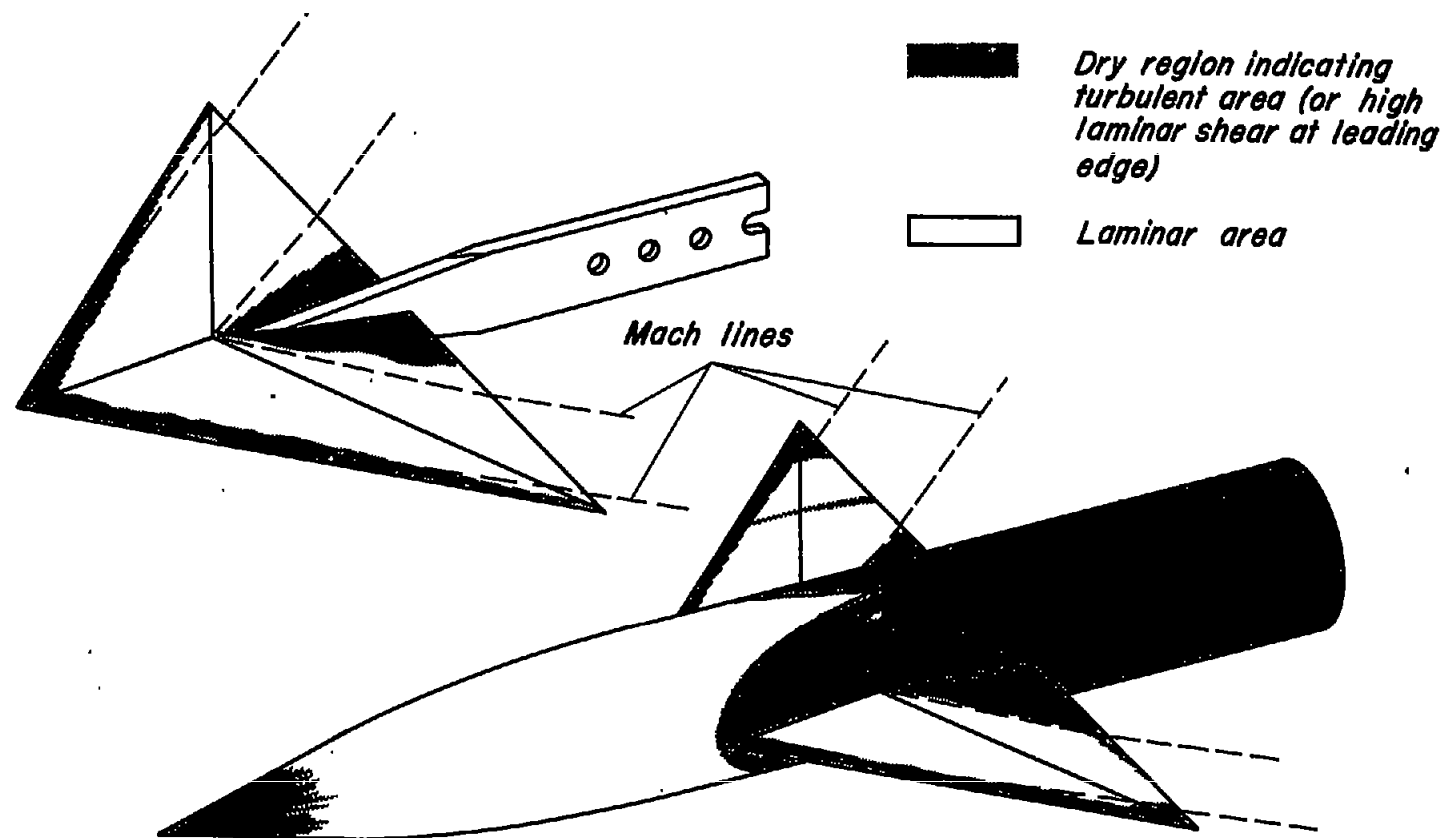


Figure 9.- Sketches of boundary patterns made from liquid film studies of wing 6 and combination W_6B at $M=1.5$, $\alpha=0^\circ$.

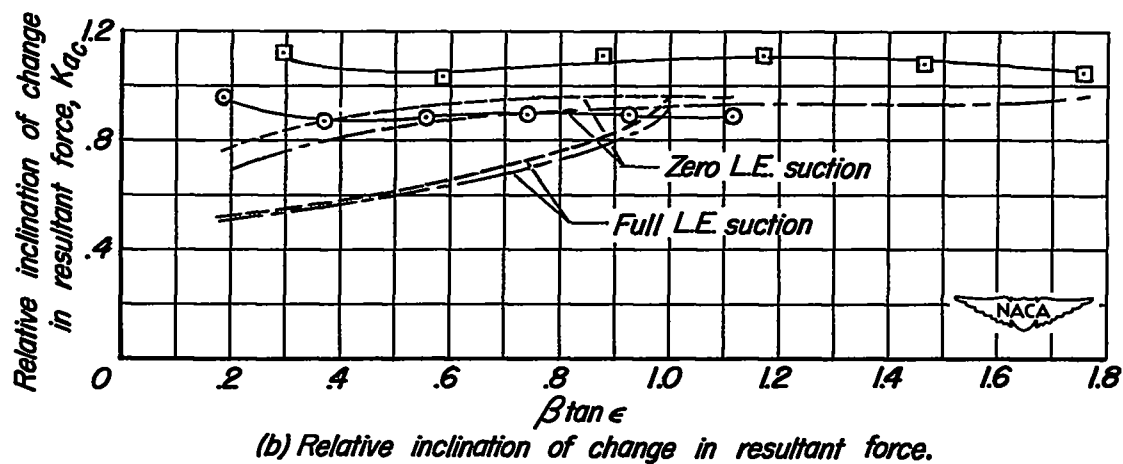
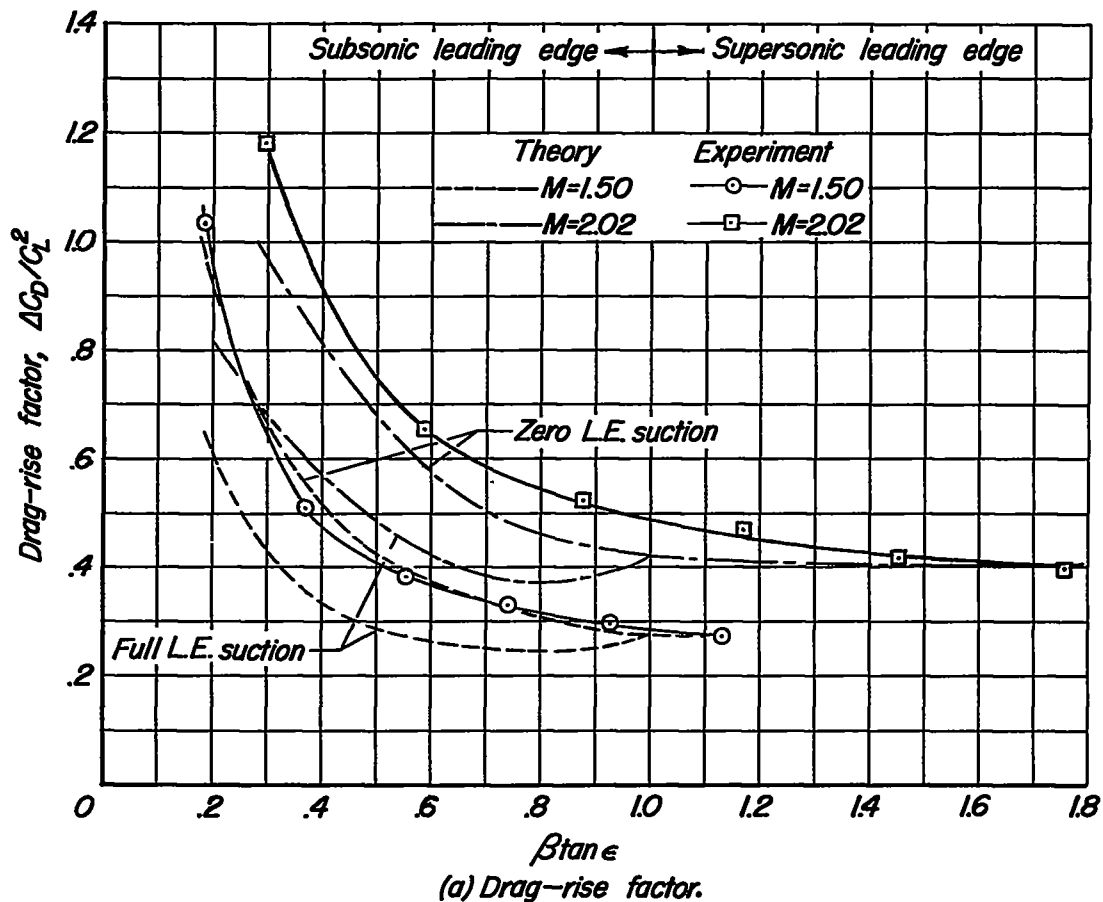


Figure 10.—Drag-rise characteristics of wing-body combinations.

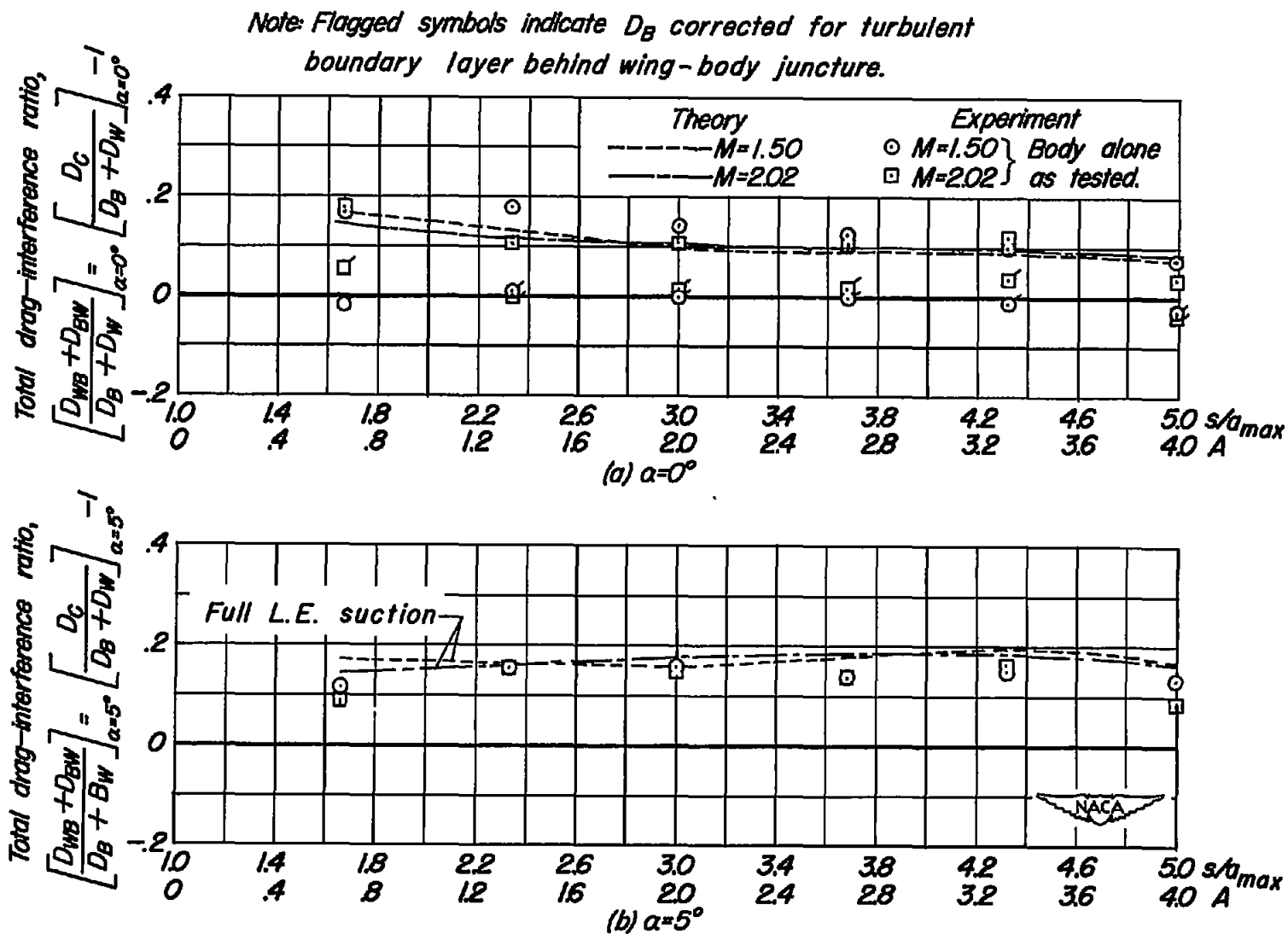


Figure 11.—Total drag-interference ratio at $M=1.50$ and $M=2.02$.